Quantum-Beam-Induced Phenomena in Chlorinated Resists:

Reaction Mechanisms and Applications to Advanced Technologies

塩素系レジストの量子ビーム誘起反応：
反応機構の解明と先端技術への応用

February 2012

Research on High Quality Beam Science
Major in Pure and Applied Physics
Graduate School of Advanced Science and Engineering
Waseda University

Tomoko GOWA OYAMA

Contents

Introduction

1

Background and Motivation

Semiconductor devices have become integral to electronic products that support today's science and technology. Their capabilities such as processing speed and memory capacity are dependent on the density of components that can be patterned onto a chip. Because high integration requires fine pattering techniques, lithography is now one of the most strategic research areas in both academia and industry.

Semiconductor devices are fabricated using photolithography. In this process, a photo-sensitive material, called "resist", is used to transfer complex circuit patterns onto wafer substrates. The semiconductor industry has repeatedly attempted to use shorter wavelengths of exposure light for lithographic patterning, in order to achieve higher resolution for higher integration. However, the current photolithography is now reaching the resolution limit. Instead of UV light, highly-controlled artificial radiation called "quantum beams" have been proposed for mass-production in the near future. At the same time, the perspective for understanding and controlling reactions in resists should shift from photochemistry to radiation chemistry.

1.1 Lithography

The basic procedure of lithography is schematically shown in Fig. 1.1. The process that uses light to transfer patterns onto a substrate is called photolithography. A photo-sensitive material, called "resist", is coated on the substrate and patterned by light via chemical reactions. The pattern-formed resist is used as a mask to protect selected areas, and subsequently, the patterns are transferred to the substrate by an etching process. This cycle is repeated about 50 times to obtain the complex patterns required for semiconductor devices.

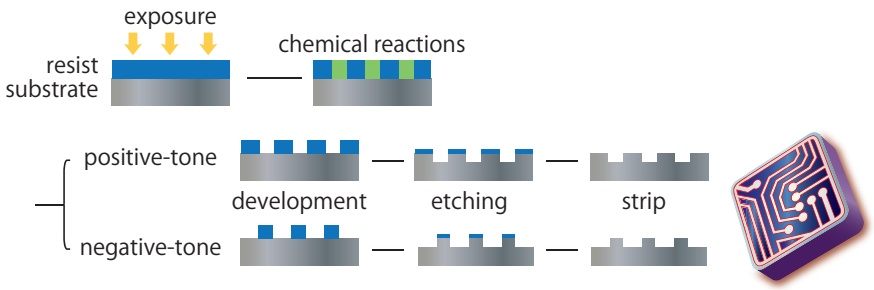

Fig. 1.1 | Typical steps in lithography process.

In 1975, Intel's co-founder G. E. Moore predicted that the number of transistors per integrated circuit (IC) would be doubled every two years at minimum cost.[1,2] In accordance with the so-called "Moore's law", high integration has been achieved with the development of pattering technology. In part, Moore's law has been used to predict and define the long-term strategy for research and development in the semiconductor industry.

The critical dimension (CD) of photolithography is limited by the exposure wavelength (λ) as following formula, where k_1 denotes the process-related factor and NA denotes the numerical aperture of the lens that is used to capture the pattern:[4]

$$CD = k_1 \cdot \frac{\lambda}{NA} \tag{1.1}$$

In order to achieve higher resolution for higher integration, the semiconductor industry has repeatedly attempted to use shorter wavelengths in the exposure process. Until the 1980s, the g-line (436 nm), h-line (405 nm), and i-line (365 nm) emitted from mercury lamps had been used for patterning. Subsequently, KrF (248 nm) and ArF (193 nm) excimer lasers have propelled miniaturization of the fabrication feature sizes. Recently, the liquid immersion technique has extended the patterning resolution below 50 nm; this process enhances resolution by filling the gap between the lens and the wafer with a liquid having high refractive index.

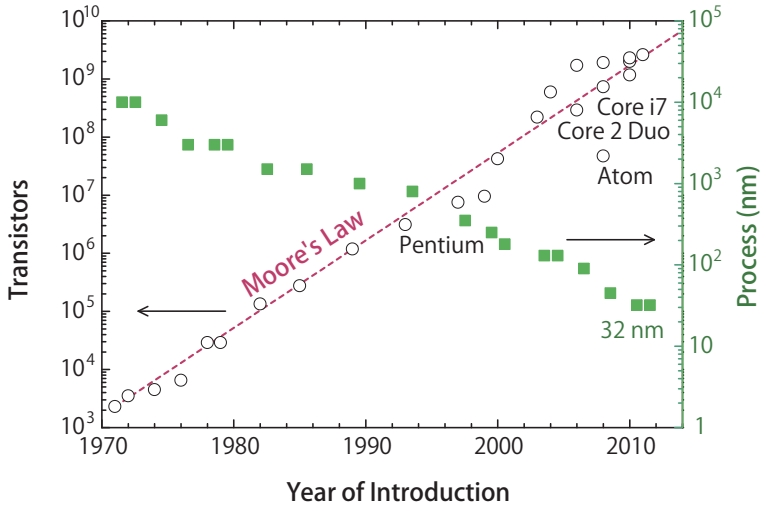

Fig. 1.2 | Evolution of Intel processors and Moore's law.[3)]

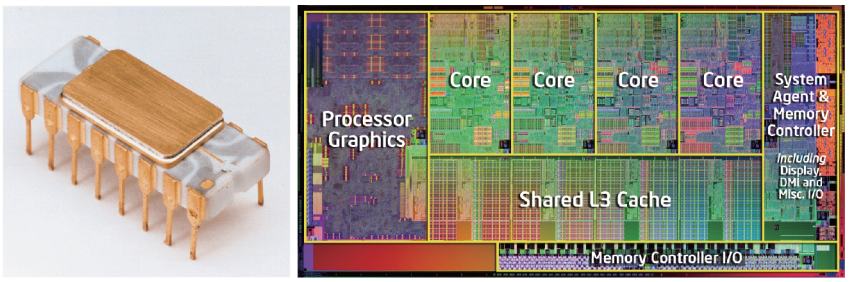

Fig. 1.3 | First commercial microprocessor Intel 4004 (740 kHz / 10 µm) in 1971, and Intel Core i7 processor (3.4 GHz / 32 nm) in 2010. (Courtesy of Intel)

As of 2011, ArF excimer lasers coupled with the liquid immersion technique have been used to realize mass-production of central processing units (CPU) at the 32 nm node (*e.g.*, the Intel Core i7).

1.2 Transition from Photochemistry to Radiation Chemistry

Research in the semiconductor industry continues to focus on the next technological innovations at a rapid pace. The International Technology Roadmap for Semiconductors (ITRS)[5)] defines two main approaches for future developments: further miniaturization ("More Moore") and functional diversification ("More than Moore"). For example, Intel announced in May 2011 that they have planned on introducing a three-dimensional (3-D) fabrication technique called "3-D Tri-Gate technology" into high-volume manufacturing of transistors at the 22 nm node.[3,6)]

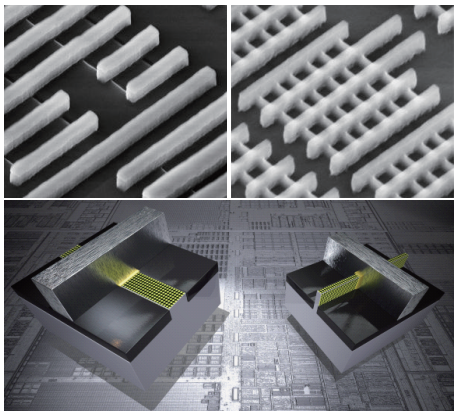

Fig. 1.4 | Intel's 32 nm planer (left) and 22 nm 3-D Tri-Gate transistors that are named for the three sides of the gate. (Courtesy of Intel)

However, the current photolithography is now reaching the resolution limit. Although electron beam (EB) lithography can overcome the diffraction limit of light to achieve nano-meter resolution, the primary challenge is low throughput because of the long exposure time required for a focused EB to draw patterns directly.

Therefore, as a replacement to the ArF excimer laser, extreme ultraviolet (EUV) has been considered as the ultimate exposure source in projection lithography. The exposure wavelength for the 22 nm node and below is currently expected to be 13.5 nm. There is a significant difference between 193 nm ArF and 13.5 nm EUV. The photon energy of the 13.5 nm EUV is approximately 92 eV, which substantially exceeds the ionization potentials of the normally used resists, as shown in Fig. 1.5. That is, EUV is classified as ionizing radiation similar to EB.

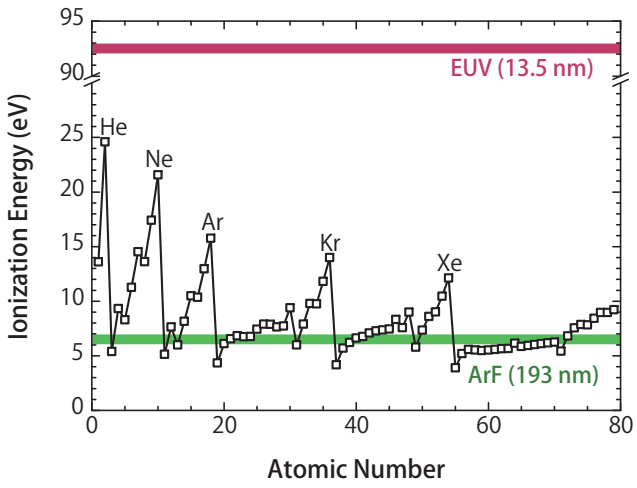

Fig. 1.5 | Periodic trend of ionization energy versus atomic number.[7)]

With the transition from light to ionizing radiation, the perspective for understanding and controlling reactions in resists should shift from photochemistry to radiation chemistry. Hence, this dissertation focuses on the reaction mechanisms in resists induced by ionizing radiations including EBs, ion beams, and EUV/soft X-rays. The radiation sources used in this study are highly-controlled artificial radiations, and they are called “quantum beams”.

1.3 Ionization Induced by Quantum Beams

Ionizing radiations eject orbital electrons from atoms or molecules in varying energy absorption processes. The pair of the produced ion (M^+) and electron (e) (geminate ion pair), occupies a space called a spur. The ejected electron loses its energy through interaction with the surrounding molecules and reaches its thermal energy level (thermalization). The charged species interact through the Coulomb force within the Onsager length, which is the distance at which the Coulomb force is equal to the thermal energy of the electron.

The concentration of the spurs is related to the linear energy transfer (LET) of the incident radiation, which is a measure of the energy transferred to the material per unit path length. For low-LET radiations such as photons and EBs, most of the spurs are isolated from each other. The thermalized electrons recombine with their parent radical cations (geminate ion recombination). In contrast, for high-LET radiations such as ion beams, the spurs overlap into a continuous track (multi-spur). Therefore, the probability of reaction with other ion pairs is increased.

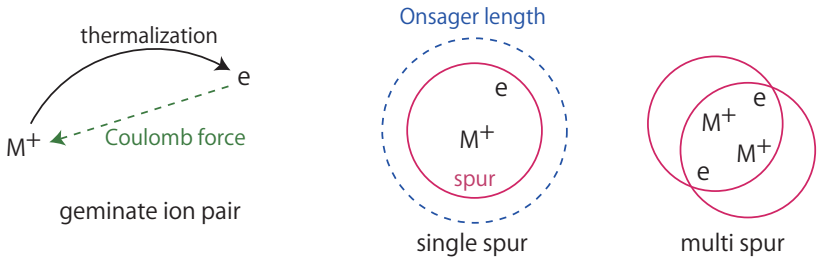

Fig. 1.6 | Schematic drawing of geminate ion pair and spurs.

The ionization and inter/intra-spur reactions occur within a very short time, as shown in Fig. 1.7. These early processes determine the chemical reactions that form the final products. Radiation chemistry in resists has been intensively studied using pulse radiolysis, which is a powerful tool for the study of short-lived intermediate species.[8–13] However, this dissertation focuses on the analysis of the final products.

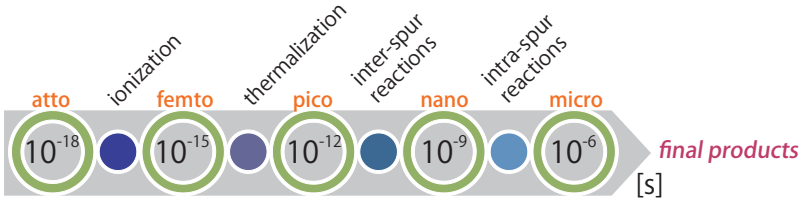

Fig. 1.7 | Time-scale of radiation-induced reactions.

1.4 Resists

Resist materials play an important role in lithography. There are strict requirements for resist performance; these include high resolution, high sensitivity, low line edge roughness (LER), and high etching resistance. High sensitivity is essential for mass-production of electronic devices, because exposure light intensity and resist sensitivity are complementary. LER must be reduced for precise and error-free fabrication. For the 22 nm node, a sensitivity higher than 10 mJ cm^{-2} and an LER that is less than 1.5 nm are required.

Resists are classified into two types based on their dissolution property after the exposure: positive-tone and negative-tone.[14] The light-exposed areas of a positive-tone resist become soluble to the developer, while for the negative-tone resist, the light-exposed areas become insoluble.

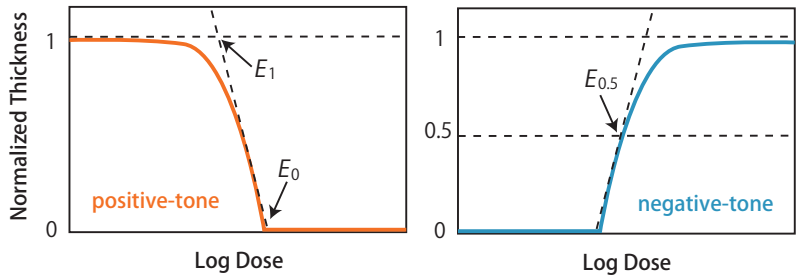

Fig. 1.8 | Sensitivity curves of resists and definitions of sensitivity and contrast.

The resist sensitivity is evaluated from the sensitivity curve (shown in Fig. 1.8) which indicates the normalized remaining resist thickness after development. The sensitivity of positive-tone resists is defined as the dose-to-clear (E_0), which is the dose required to completely develop the resist film. For negative-tone resists, the sensitivity is defined as the dose at which the curve is at 50% of the film thickness ($E_{0.5}$). The resist sensitivities are evaluated using E_0 and $E_{0.5}$ in this dissertation. However, it should be noted that the dose actually required for fabrication is dependent on the feature size (dose-to-size, E_{size}).

The resist contrast (γ) is another important factor in the evaluation of resist performance. It is defined as the tangent of the sensitivity curve slope. A higher contrast resist has higher vertical resolution and better sidewall profiles.

$$\gamma = \left| \log_{10} \left(\frac{E_1}{E_0} \right) \right|^{-1} \tag{1.2}$$

Poly(methyl methacrylate)

Poly(methyl methacrylate) (PMMA) is a well-known positive-tone resist for ionizing sources such as EB and X-rays. PMMA undergoes main-chain scission upon irradiation, and its detailed reaction mechanisms have been extensively studied. The resolution of PMMA is below 10 nm,[15] and even as high as 3 nm under special conditions.[16] However, its low sensitivity and poor etching resistance are huge drawbacks for practical lithography. It has been reported that the sensitivity for a 20 keV EB is in the 10^{-4} C cm^{-2} range, that is, several J cm^{-2}.[17,18]

Chemically amplified resists

A breakthrough enhancement of resist sensitivity has been achieved by the concept of "chemical amplification", proposed by H. Ito *et al.* in 1982.[19,20] Chemically amplified (CA) resists comprise a polymer resin and a photoacid generator (PAG)/ photobase generator (PBG). The acids/bases generated by the irradiation catalyze hundreds of deprotection events during the post-exposure bake (PEB), thereby resulting in an amplified polarity change in the polymer.[14,21] In general, poly(hydroxy styrene) (PHS) is applied as the base polymer for CA resists, and the photo- and radiation-induced reaction mechanisms of such resists have been intensively studied.[13] In addition to high sensitivity, PHS-based CA resists have high etching resistance due to the presence of the phenyl groups.

CA resists are considered to be the most promising candidates for high-volume manufacturing with EUV lithography. For 13.5 nm EUV exposure, sensitivities of 10–20 mJ cm^{-2} have been achieved with PHS-based CA resists at a sub-30 nm resolution.[13] However, it has been known that the sensitivity, resolution, and LER of CA resists are mutually exclusive in relation to each other, *i.e.*, they are linked by a trade-off relationship.[13]

ZEP resists

Among the various commercially available resists, ZEP resists (ZEP520A and ZEP-7000) manufactured by ZEON (Tokyo, Japan) are commonly used for practical EB lithography. These resists are positive-tone resists with excellent spatial resolutions,

and their performance is comparable to that of PMMA. Furthermore, the sensitivities of ZEP resists are much higher than that of PMMA even though ZEP resists are non-CA resists.[22,23] ZEP resists consist of 1:1 copolymer of α-chloromethacrylate and α-methylstyrene with different molecular weights (M_w of ZEP520A: ~57,000, ZEP7000: ~340,000).[23–26] The structure of ZEP is similar to that of the combination of PMMA and polystyrene, and the etching resistance is much better than that of PMMA due to the presence of the phenyl groups.

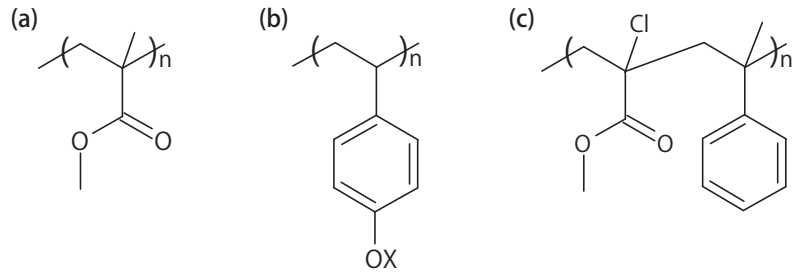

Fig. 1.9 | Structures of (a) PMMA, (b) PHS-based resist, and (c) ZEP.

Table 1.1 | Property comparison of ZEP with typical resists.

	PMMA	PHS-based CA	ZEP
Sensitivity	poor	excellent	excellent
Resolution	excellent	good	excellent
Etching resistance	poor	good	good

Although ZEP resists have been practically used as EB resists for more than 20 years since the 1990s, their reaction mechanisms have not yet been fully understood. The causes underlying the excellent balance between high resolution and high sensitivity in ZEP resists have been considered an interesting research topic. This dissertation focuses on the reaction mechanisms in ZEP resists that are induced by quantum beams such as EBs, ion beams, and EUV/soft X-rays.

2

Outline of Dissertation

This dissertation is organized in two parts: study of the mechanisms of quantum-beam-induced reactions in chlorinated polymers (Part I), and applications to several advanced technologies by controlling these reactions (Part II).

Part I: Mechanisms of Quantum-Beam-Induced Reactions

1. Decomposition Mechanisms in Chlorinated Resists

Chapter 1 investigates EB-induced decomposition mechanisms in ZEP resists by analyzing the obtained final products. The reason for the excellent balance between high resolution and high sensitivity in ZEP resists is discussed in this chapter.

2. Positive-Negative Inversion Induced by High-Dose Irradiation

Chapter 2 describes the mechanisms of positive-negative inversion of ZEP resists; that is the phenomenon through which positive-tone resists change into negative-tone by high-dose irradiation.

3. Linear Energy Transfer Effects on Resist Performance

Chapter 3 discusses the dependence of linear energy transfer (LET) on the induced reactions by comparing sensitivities of ZEP resists upon irradiation by low-LET EBs and high-LET ion beams.

4. Absorption Properties and Resist Performance

Chapter 4 describes the wavelength dependence of the resist performance, which is investigated using monochromated EUV/soft X-rays. Moreover, the resist sensitivities are discussed in terms of the absorbed dose.

Part II: Applications to Advanced Technologies

1. Micro/Nanofabrication Technique Using Positive-Negative Inversion

Chapter 1 demonstrates a novel fabrication technique, named “nanobead from nanocup”. By applying the positive-negative inversion and energy deposition distribution of an irradiating beam, the desired micro/nanostructures such as nanomembranes and nanowires can be successfully obtained.

2. Evaluation of Resist Performance for Next-Generation Lithography

Chapter 2 presents the prediction strategy for resist sensitivities. This method provides a guideline for the selection and development of high sensitivity resists for next-generation EUV/soft X-ray lithography.

3. X-ray Imaging with Resists for Elemental Mapping

Chapter 3 proposes the use of ZEP resists as high resolution recording film for X-ray imaging that can enable elemental mapping. The X-ray imaging of nanoparticles is reported.

Concluding Remarks

Finally, the key contributions of this dissertation and future plans are summarized in the concluding remarks.

Part I

Mechanisms of Quantum-Beam-Induced Reactions

1

Decomposition Mechanisms in Chlorinated Resists

ZEP resists (1:1 copolymer of α-chloromethacrylate and α-methylstyrene, ZEON) are positive-tone resists that are used for electron beam (EB) lithography, and are known for their high sensitivity and high resolution. In this chapter, we examine ZEP resists that are irradiated with 100 kV EB, and further, we analyze the degradation mechanisms using gel permeation chromatography (GPC), UV-visible (UV-vis) spectroscopy, Fourier transform infrared (FT-IR) spectroscopy, X-ray photoelectron spectroscopy (XPS), nuclear magnetic resonance (NMR) spectroscopy, and pulse radiolysis.

Subsequent to the analysis, it is confirmed that chlorine atoms easily dissociate as Cl^- ions (dissociative electron attachment, DEA), and ZEP resists undergo β-scission. Multiple reaction channels are considered for the main-chain scission, including DEA and charge transfer (CT) complex between phenyl radical cations and Cl^- ions. The reason for the excellent balance between high resolution and high sensitivity in ZEP resists is discussed in this chapter.

1.1 Introduction

ZEP resists (ZEON) comprise a 1:1 copolymer of α-chloromethacrylate and α-methylstyrene with different molecular weights (M_w of ZEP520A: ~57,000, ZEP7000: ~340,000).[23–26] It has been reported that ZEP resists have an excellent spatial resolution better than 10 nm, and this value is comparable to that of PMMA. Furthermore, the sensitivities of ZEP resists are much higher than that of PMMA, even though they are non-CA resists.[22,23] However, the radiation-induced degradation mechanisms of ZEP resists have not yet been fully clarified.

In this chapter, we examine ZEP resists irradiated with a 100 kV EB. The induced reactions are evaluated using GPC, UV-vis spectroscopy, FT-IR spectroscopy, XPS, NMR spectroscopy, and pulse radiolysis. Subsequently, we discuss the reason for the excellent balance between high resolution and high sensitivity.

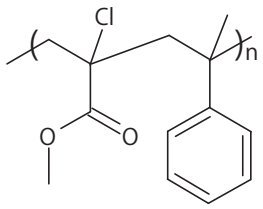

Fig. 1.1 | Reported structure of ZEP resists.[23,24]

1.2 Methods

Sample preparation of ZEP resists

For sensitivity measurement, spin-coated film samples were prepared based on the conditions recommended by ZEON. The following procedure is adopted throughout this dissertation unless otherwise stated. All the processes were performed under ambient conditions at 25 °C.

- Spin-coating: 3000 rpm for 60 s, on Si wafers
- Pre-bake: 180 °C, 180 s
- Development:
  ZEP520A: ZED-N50 (n-amyl acetate 100%), 60 s
  ZEP7000: ZED-500 (3-pentanone 50%, diethyl malonate 50%), 60 s
- Rinse:
  ZEP520A: ZMD-B (methyl isobutyl ketone 89%, isopropyl alcohol 11%), 10 s
  ZEP7000: ZMD-D (methyl isobutyl ketone >99%), 10 s

The thicknesses of ZEP520A and ZEP7000 films after the pre-bake process were approximately 350 and 150 nm, respectively. For GPC, FT-IR, and NMR analyses, the ZEP resists on Si wafers (spin-coated at 1000 rpm for 60 s, approx. 500 nm thick) were extracted using chloroform. Subsequently, the chloroform was removed by rotary evaporation under reduced pressure. For FT-IR spectroscopy, irradiated samples were directly scraped from the wafers.

EB irradiation

The irradiation was carried out with EB-ENGINE® (Hamamatsu Photonics) under N_2 gas flow conditions (monitored O_2 < 100 ppm) at 25 °C. The selected acceleration voltage was 100 kV, and a large (ϕ 10 mm) and uniform EB scanned the sample surface with a speed of 100 mm s^{-1}. The EB passed through a beryllium window and nitrogen-filled space before irradiating the sample. The energy of the EB at the sample surface was calculated to be about 90 keV, by using the Monte Carlo code EGS5.[27)]

Measurements

The thicknesses of the spin-coated and developed resist samples were measured using an atomic force microscope (AFM, SPI3800: SII NanoTechnology).

The molecular weight of the degraded ZEP520A was analyzed using a SHIMADZU LC-10A GPC system (composed of SCL-10A VP, LC-10A VP, and CTO-10A VP) and a UV-detector (SPD-M10A VP, monitored at λ = 260 nm). The measurement was conducted at 40 °C using a 7.5 mm ID × 300 mm Shodex KF 805L (×2) with KF-G columns using THF (Kishida Chemical, GPC grade) as an eluent at a flow rate of 1.0 mL min^{-1}, and the molecular weight was calculated from the calibration curve for standardized polystyrene.

The absorbance of ZEP resists spin-coated on quartz wafers was measured by UV-vis spectroscopy (V-630: JASCO) with a scan speed of 20 nm min^{-1}. FT-IR spectroscopy was carried out using Nicolet 6700 (Thermo Fisher Scientific) with a single-reflection diamond ATR attachment (Smart Orbit). The spectra were collected at a resolution of 2 cm^{-1} and averaged over 128 scans.

The changes in the elemental compositions of the resists were evaluated by XPS (JPS-9010TR: JEOL) with a MgKα source (<5×10^{-7} Pa).

^{1}H NMR spectra were recorded on a JEOL JMN-400 spectrometer. ^{13}C NMR, distortionless enhancement by polarization transfer (DEPT) of ^{13}C NMR, and ^{1}H–^{13}C heteronuclear multiple-quantum correlation (HMQC) and heteronuclear multiple-bond correlation (HMBC) spectra were recorded on a Bruker BioSpin AVANCE III 700 spectrometer. All the NMR measurements were conducted in $CDCl_3$ with tetramethylsilane (TMS) as an internal standard.

1.3 Results and Discussion

1.3.1 Decrease in molecular weight

First, the sensitivities of ZEP resists to the 100 kV EB were evaluated using the spin-coated film samples. Fig 1.2 shows the obtained sensitivity curves, which indicate the normalized remaining resist thickness for the exposure dose. The sensitivities (E_0, the doses required to completely develop the resists) were approximately 84 μC cm^{-2} for ZEP520A and 6.0 μC cm^{-2} for ZEP7000.

The sensitivity difference between ZEP520A and ZEP7000 may be due to the different developers used in the experiment. The molecular weight of ZEP7000 is higher than that of ZEP520A.[25,26] Stronger developers can be applied for resists with high molecular weight, therefore, the sensitivity of ZEP7000 could be made higher than that of ZEP520A with suitable development processes.

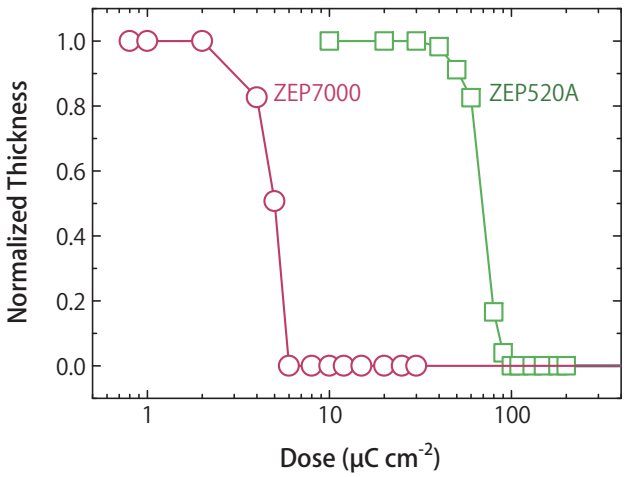

Fig. 1.2 | Sensitivity curves of ZEP resists for 100 kV EB under N_2 gas flow conditions (approx. 90 keV at the sample surface).

The molecular weight of ZEP520A was evaluated using GPC. For the nonirradiated (blank) sample, the M_w and the polydispersity index (PDI = M_w/M_n) were approximately 61,000 and 2.2, respectively. The decomposition of ZEP520A was clearly indicated from the GPC curves, shown in Fig 1.3, which shifted toward lower molecular weights in response to the irradiation dose. It was speculated that ZEP520A does not undergo crosslinking, because no peak was appeared at an elution time of around 10 min, which is the high-molecular-weight exclusion limit of the columns used in the experiment. The values of the PDI remained around 2, and this result indicates the random chain scission of ZEP resists.

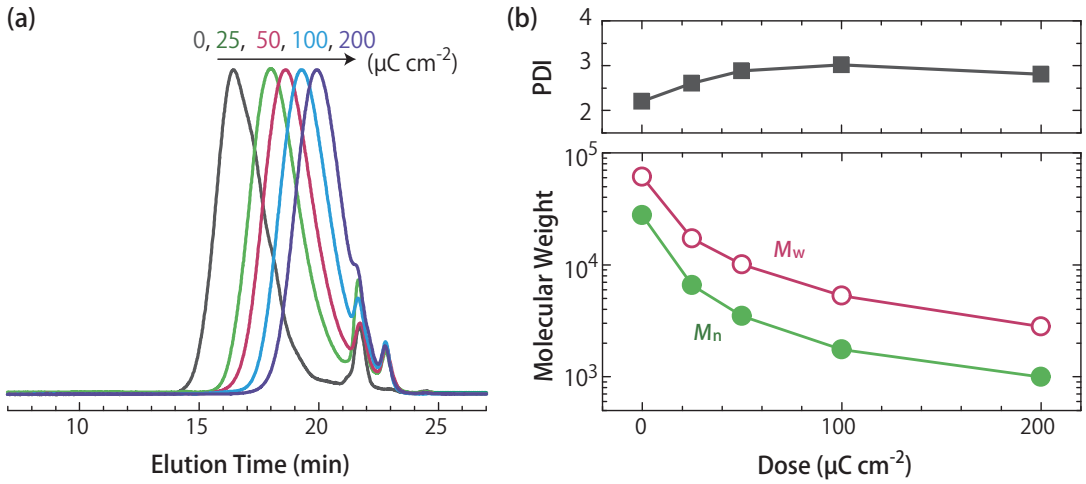

Fig. 1.3 | (a) GPC curves of blank and EB-irradiated ZEP520A and (b) calculated molecular weight and PDI.

1.3.2 Structural transitions

UV-vis spectroscopy

The absorbance of ZEP resists spin-coated on quartz wafers was measured by UV-vis spectroscopy. As shown in Fig. 1.4, the absorbance at around 190–300 nm was increased by irradiation as compared with that of the blank sample. This increase in absorbance is assigned to unsaturated bonds including C=C double bonds and produced ketones (C=O). Similar results were also obtained for ZEP7000.

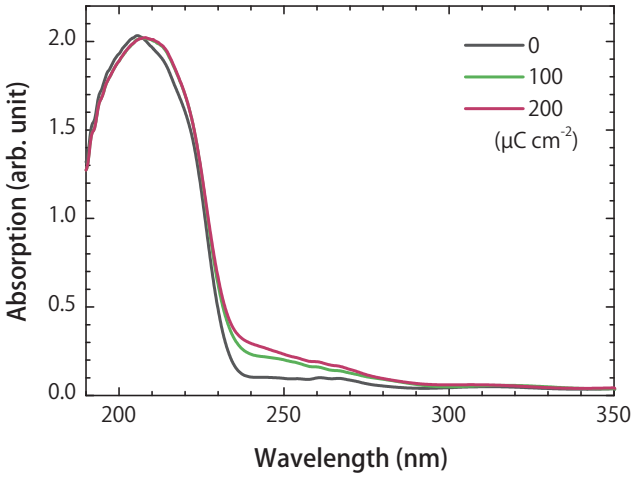

Fig. 1.4 | UV-vis spectra of ZEP520A before and after the 100 kV EB irradiation.

FT-IR spectroscopy

Fig. 1.5 shows the obtained FT-IR spectra for ZEP520A. It was difficult to evaluate detailed chemical reactions from these spectra because most of the peaks overlapped with each other.

However, an interesting transition was observed with the ester C=O bonds, which absorbed at two wavenumbers (1750 and 1725 cm^{-1}). This is attributed to the rotational isomerism (field effect). When the chlorine atom is near the carbonyl oxygen, the C=O absorption peak shifts to a higher wavenumber (1750 cm^{-1}).[28] However, this peak decreased in response to the irradiation dose. The result indicates that the C–Cl bonds were decomposed by irradiation. Similar changes were observed with the doublet absorption peaks of C-O (1240 and 1200 cm^{-1}).

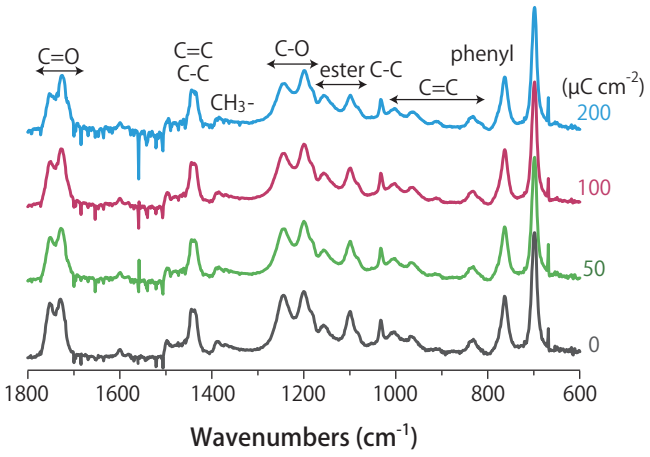

Fig. 1.5 | FT-IR spectra of ZEP520A before and after the 100 kV EB irradiation.

XPS

The change in elemental compositions was evaluated by XPS. Although only carbon (C), chlorine (Cl), and oxygen (O) were detected for the blank samples, nitrogen (N) was also found for the irradiated ones. The ratios of O/C, Cl/C, and N/C were evaluated from the peak areas and the sensitivity factors for each element. The compositions of the blank samples were consistent with those of the reported structures of ZEP resists, *i.e.*, 1:1 copolymer of α-chloromethacrylate and α-methylstyrene.[23]

The intensities of O and N were increased by the irradiation. It was speculated that oxide and amine groups are formed due to the reaction between the induced radicals and ambient gas during the irradiation or after exposure to air. A distinct decrease was observed for Cl in response to the irradiation dose, as also suggested by the results of FT-IR spectroscopy.

Table 1.1 | Ratios of O/C, Cl/C, and N/C of ZEP resists evaluated by XPS.

Dose ($\mu C\ cm^{-2}$)	O/C		Cl/C		N/C	
	ZEP520A	ZEP7000	ZEP520A	ZEP7000	ZEP520A	ZEP7000
0[a)]	0.15	0.15	0.077	0.077	0	0
0[b)]	0.16	0.16	0.086	0.086	N.D.	N.D.
50	0.21	0.19	0.066	0.060	0.020	0.020
100	0.24	0.24	0.065	0.059	0.036	0.040

a) reported b) measured N.D. : not detected

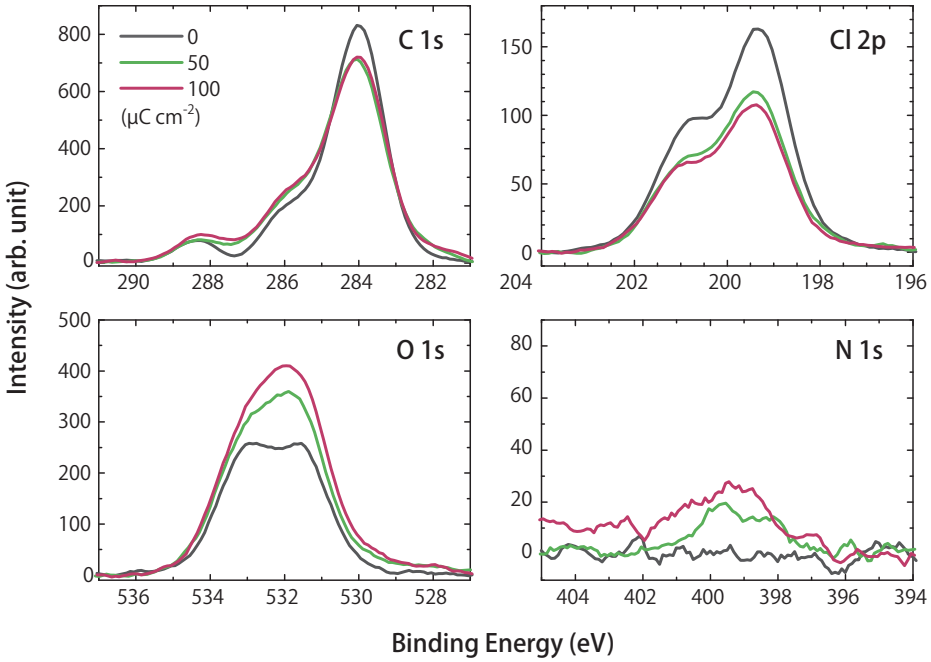

Fig. 1.6 | XPS spectra of ZEP520A before and after the 100 kV EB irradiation.

The typical XPS spectra of each element in ZEP520A are shown in Fig. 1.6. The Cl 2p spectra include a Cl doublet (201 and 199.3 eV) and weak peaks of a Cl^- 2p doublet (198.8 and 197.3 eV).[29)] Most of the Cl^- anions produced during the irradiation would evaporate as HCl due to recombination with protons.

In the O 1s spectra, there are two peaks at 533 and 531.4 eV, and these are assigned to O–C and O=C bonds, respectively.[30,31)] Their ratio in the blank sample is nearly 1:1, reflecting the ester bonds. The increasing number of O=C bonds would be due to the ketones produced during irradiation, as suggested by the UV-vis spectra. In addition, the N 1s spectra suggest the generation of amines including $CO–NH_2$ (401 eV), C=N (399.5 eV), and $C–NH_2$ (398.5 eV).[30)]

In view of these results, the C 1s spectrum of the blank samples can be separated into five components: C–C (284 eV, including C–H and C=C), C–O (285.5 eV), C–Cl (286.2 eV), O–C=O (288.3 eV), and π–π* transitions due to conjugation (291 eV).[30–32] After the irradiation, the new components are expected to appear as discussed above. Although C=O (287.3 eV) and C=N (286.6 eV) can be separated, CO–NH_2 and C–NH_2 are hardly distinguished from the O–C=O and C–O peaks.[30]

NMR spectroscopy

The detailed structural transition by EB irradiation was investigated with ^{1}H NMR spectra, as shown in Fig. 1.7. The signal assignments were performed by DEPT of ^{13}C NMR, ^{1}H–^{13}C HMQC, and ^{1}H–^{13}C HMBC of the blank sample.

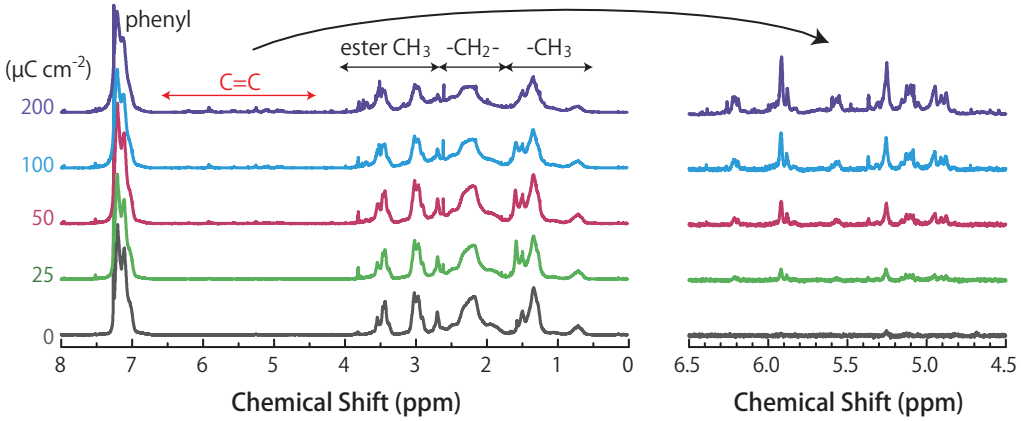

Fig. 1.7 | ^{1}H NMR spectra of ZEP520A before and after the 100 kV EB irradiation.

The main-chain –CH_2– (1.7–2.5 ppm) and α–CH_3 (0.6–1.7 ppm) decreased with increasing irradiation dose. For doses higher than 200 μC cm^{-2}, ester CH_3 (2.5–3.8 ppm) began to decrease. This result suggests the cleavage of ester side chains. On the other hand, peaks assigned to C=C double bonds (4.8–6.5 ppm) increased after the irradiation. For an irradiation dose of 200 μC cm^{-2}, the spin-lattice relaxation time (T_1) of the generated double bonds at 5.9 ppm (0.93 s) is much longer than that of α–CH_3 at 0.71 ppm (0.24 s). This result indicates that the C=C double bonds were generated at the terminal of the polymer chain.

The HMQC and HMBC spectra of the sample irradiated with 200 μC cm^{-2} were obtained for detailed analysis. The HMQC spectra show one-bond correlations between protons and carbons. As shown in Fig. 1.8, six ^{13}C–^{1}H cross peaks were observed between three peaks of ^{1}H (4.8–6.5 ppm) and two peaks of ^{13}C (120 and 124 ppm). These peaks indicate that protons are directly bonded to the terminal double bonds as –CH=CH_2.

The position of the terminal –CH=CH_2 bonds was investigated using the HMBC spectra, which shows correlations between protons and carbons separated by two or three chemical bonds.

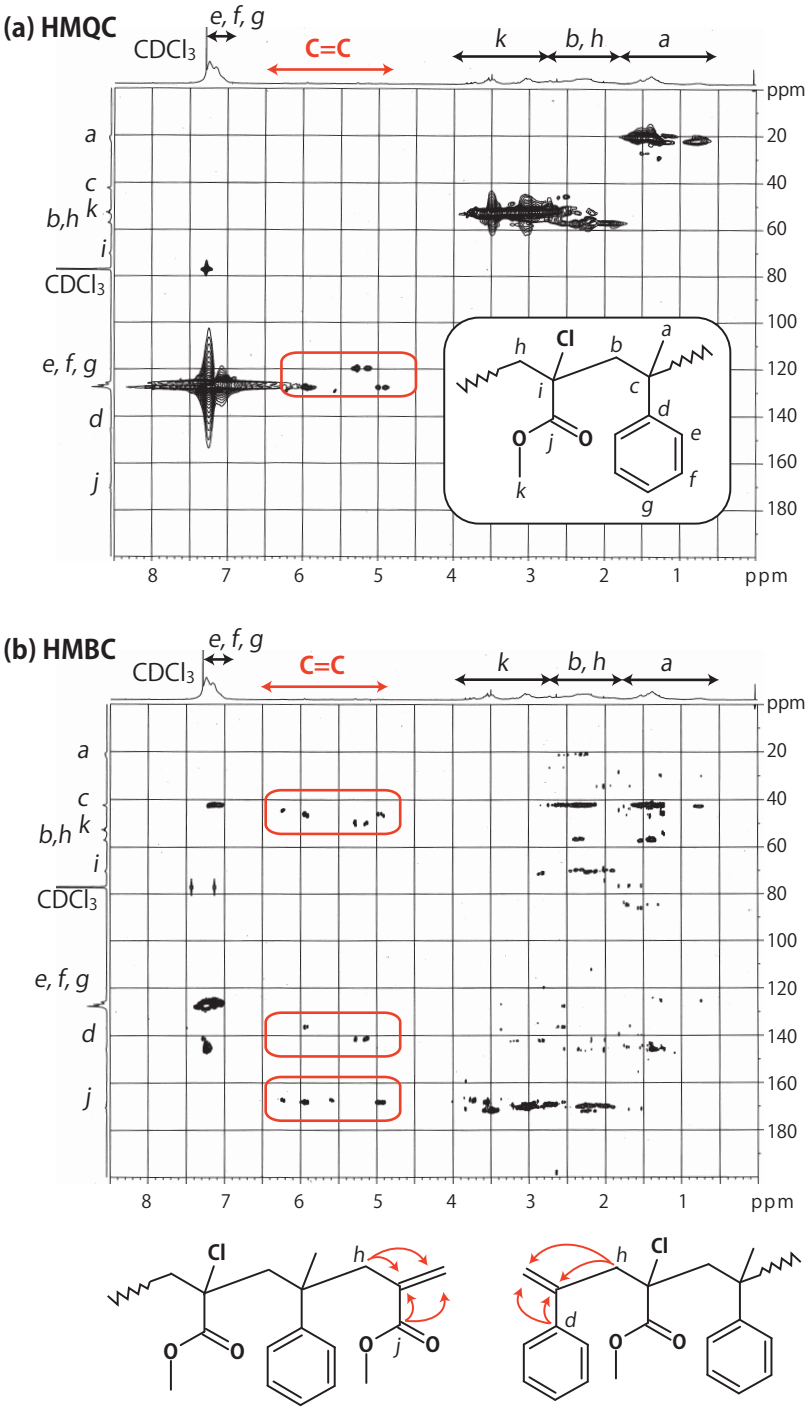

Fig. 1.8 | ^{1}H–^{13}C HMQC and HMBC spectra of ZEP520A for an irradiation dose of 200 µC cm^{-2} and the peak assignments.

The chemical shifts around 170, 140, and 45 ppm of ^{13}C correlated with 4.8–6.5 ppm of ^{1}H. The results suggest that the –CH=CH_2 bonds were generated in the neighborhood of carbon-j, d, and h. Hence, it was confirmed that ZEP underwent main-chain scission, and terminal C=C double bonds were generated at both αClMA and αMS units.

1.3.3 Efficiency of main-chain scission

The G-value (events per 100 eV) of the main-chain scission (G(s)) was calculated using the Alexander-Charlesby-Ross equation given below, where M_{n0} denotes the M_n of the blank sample and D denotes the absorbed dose given in Gy (= J kg^{-1}).[33,34]

$$\frac{1}{M_n} = \frac{1}{M_{n0}} + 1.04 \times 10^{-10} G(s) D \tag{1.1}$$

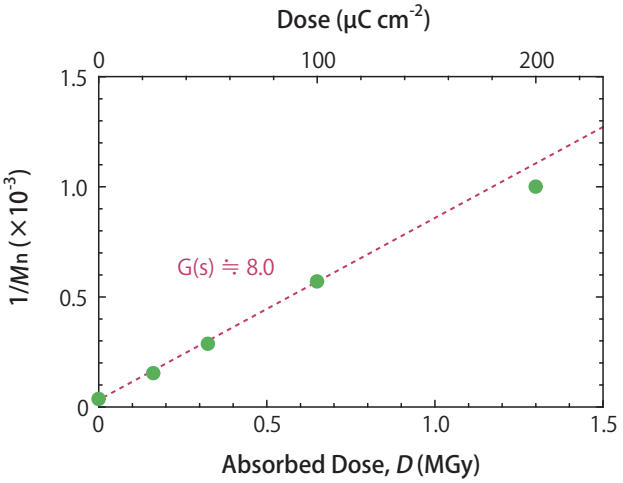

Fig. 1.9 | $1/M_n$ versus absorbed dose D.

From Eq.(1.1), G(s) was evaluated with the slope of the approximated straight line shown in Fig. 1.9. The D value was calculated using the approximate density of ZEP520A (1.6 g cm^{-3}) and the LET was simulated using the Monte Carlo code EGS5,[27] in consideration of the decay of EB energy caused by the beryllium window and the nitrogen-filled space between the window and the sample, and backscattered electrons from the Si wafer. Subsequently, the EB energy was calculated to be about 90 keV at the sample surface, and 100 μC cm^{-2} irradiation corresponded to about 650 kGy.

For lower doses (≤100 μC cm^{-2}), the plots were well approximated by a straight line. Consequently, G(s) was estimated to be approximately 8.0. This value is very large in comparison with the G(s) value of PMMA, which is reported to be around

2.[35–37] The plot for the irradiation dose of 200 μC cm^{-2} reflects the ester side-chain cleavages as suggested by the ^{1}H-NMR spectra in Fig 1.7.

1.3.4 Decomposition mechanisms of ZEP resists

From the above results, multiple reaction channels can be considered for the main-chain scission in ZEP resists.

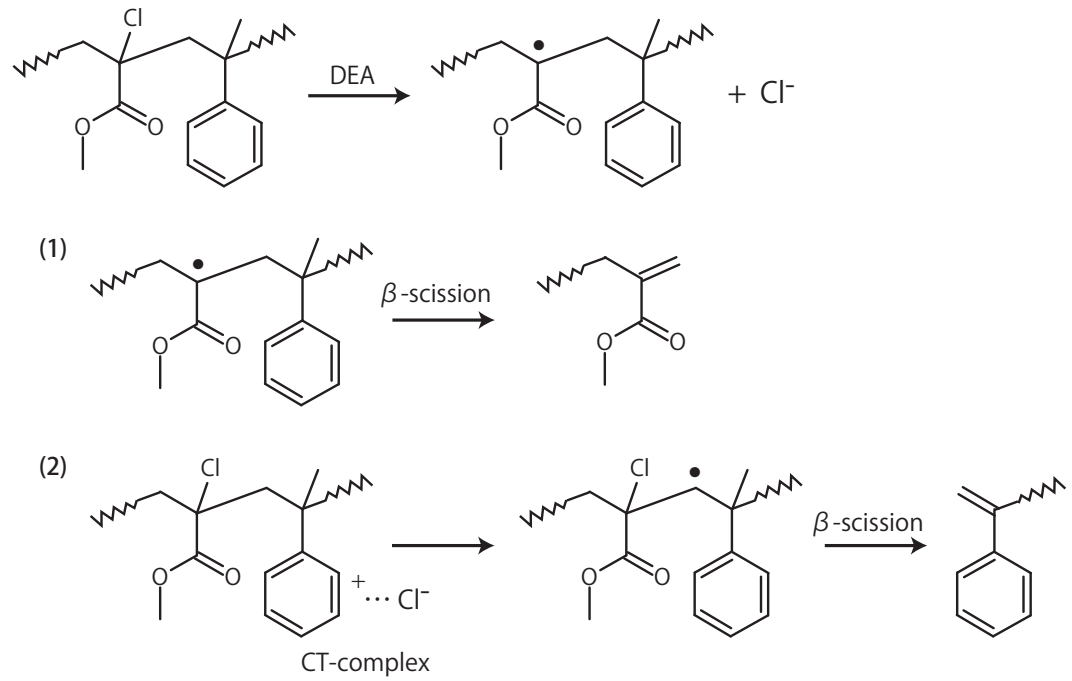

Fig. 1.10 | Decomposition mechanisms of ZEP resists.

(1) β-scission via dissociative electron attachment

According to the FT-IR and XPS analyses, the amount of chlorine atoms in the ZEP resists was decreased in response to the EB irradiation. The electron acceptor chlorine atoms would easily attach to the electrons and dissociate as Cl^- ions (dissociative electron attachment, DEA), in common with other chlorinated resists such as chloromethylated polystyrene (CMS) and chloromethylated poly-α-methylstyrene (αM-CMS).[8,9] The DEA in ZEP resists has been also suggested by our recent study in which we used pulse radiolysis.

The decrease in the length of the main-chain and the formation of the terminal double bonds at the αClMA unit were confirmed by NMR spectra. It can be concluded that the radicals generated by DEA induce β-scission in the main-chain.

(2) β-scission via charge transfer complex

It has been reported that poly(αMS) undergoes photo/radiation-induced main-chain scission effectively in chloroform ($CHCl_3$) and carbon tetrachloride (CCl_4) solutions.[38] Both photolysis and radiolysis studies show that a charge transfer (CT) complex between a phenyl ring and a chlorine atom ($Ph^+ \cdots Cl^-$) is easily formed, and this CT complex produces a β-radical which induce main-chain scission.[39–42]

The CT complex was also observed in ZEP resists in our recent pulse radiolysis study. Hence, the CT complex can also contribute to the main-chain scission of ZEP resists, and the terminal double bonds observed at the αMS unit would originate from this channel.

1.4 Summary

The decomposition mechanisms of ZEP resists were investigated in this chapter. It was confirmed that chlorine atoms easily dissociated as Cl^- ions (DEA), and ZEP resists underwent β-scission. Multiple reaction channels can be considered for the main-chain scission in ZEP, including DEA and CT complexes between phenyl rings and chlorine atoms.

The ultimate resolution of resists depends on the minimal chain length that can be broken by irradiation. The minimum interval of the possible positions that undergo β-scission is almost the same as that for PMMA. That is, ZEP resists are expected to show high resolutions comparable to that of PMMA.

The obtained results provided some clues regarding the reason for the excellent balance between the high resolution and high sensitivity of ZEP resists. The understanding of the early process of quantum-beam-induced reactions is the subject of future studies.

2

Positive-Negative Inversion Induced by High-Dose Irradiation

ZEP resists undergo main-chain scission very effectively upon EB irradiation, and the irradiated areas become soluble in developers (positive-tone). However, they become insoluble in developers after high-dose irradiation of EB (negative-tone). In this chapter, the positive-negative (P-N) inversion of ZEP resists induced by a high-dose 100 kV EB irradiation is investigated using GPC, UV-vis spectroscopy, FT-IR spectroscopy, XPS, and NMR spectroscopy.

For high-dose irradiation (>5 mC cm^{-1}), it is speculated that crosslinking becomes predominant because of the structural changes in the resists and the lower scission ratio due to the decrease in the amount of the chlorine atoms. The P-N inversion is induced as chlorine atoms are eliminated from the resists by doses of around 10 mC cm^{-2}. The content of chlorine atoms in the ZEP resists plays an important role in the determination of the scission/crosslinking probabilities.

2.1 Introduction

As described in the previous chapter, ZEP resists undergo main-chain scission very effectively upon EB irradiation. Subsequently, the irradiated areas become soluble in the developers (positive-tone). However, for high-dose irradiation the irradiated areas become insoluble in the developers, as shown in Fig. 2.1. This indicates that the dissolution property of the resists changes from positive-tone to negative-tone due to high-dose EB irradiation that is approximately 1,000 times higher than the doses discussed in Chap. 1.

It has been reported that PMMA also undergoes positive-negative (P-N) inversion upon ion beam irradiation, thereby suggesting that crosslinking reactions are induced by high-dose irradiation.[43] In this chapter, we attempt to clarify the mechanisms underlying the P-N inversion of ZEP resists using GPC, UV-vis, FT-IR, XPS, and NMR spectroscopies.

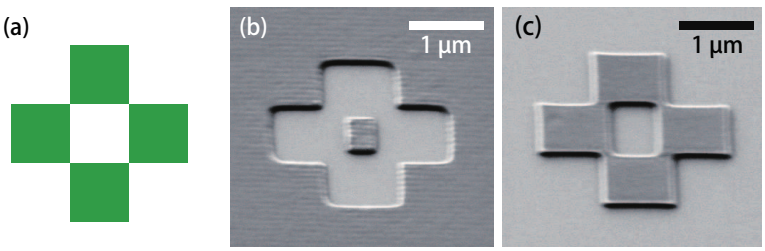

Fig. 2.1 | Four squares designed as in (a) were irradiated with (b) 0.5 and (c) 50 mC cm^{-2} by a 30 keV EB (NVision 40 with NPVE system, ZEISS). The surrounding area in (c) was irradiated with <1 mC cm^{-2}. (SEM images)

2.2 Methods

The preparation of ZEP samples, 100 kV EB irradiation, and measurements were all conducted as described in Chap. 1 (pp. 16–17).

2.3 Results and Discussion

2.3.1 Positive-negative inversion

Figure 2.2 shows the normalized resist thicknesses after development as measured by AFM. It was found that the dissolution properties changed from positive-tone to negative-tone. Although the sensitivities of ZEP520A and ZEP7000 at positive-

tone were different, both resists started to change to negative-tone at almost the same dose of around 10 mC cm^{-2}.

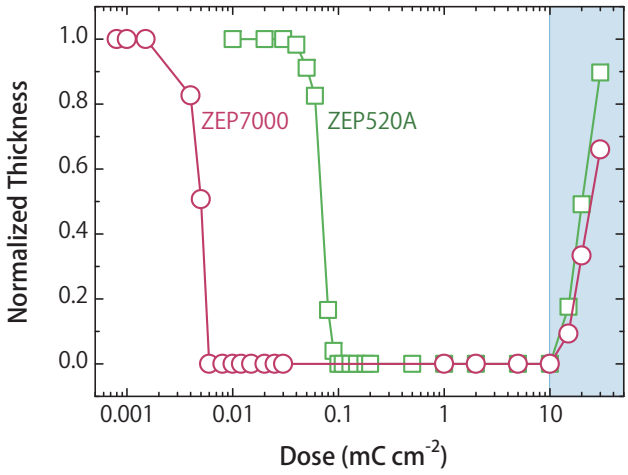

Fig. 2.2 | P-N inversion of ZEP resists induced by 100 kV EB irradiation under N_2 gas flow conditions (approx. 90 keV at the sample surface).

According to the GPC analysis shown in Fig. 2.3, the molecular weight of ZEP520A ceased to reduce for doses higher than 0.5 mC cm^{-2}. Moreover, a small recovery was observed for the samples irradiated in the range between 1 and 5 mC cm^{-2}. The samples irradiated with more than 5 mC cm^{-2} could not be measured because they dissolved poorly in THF.

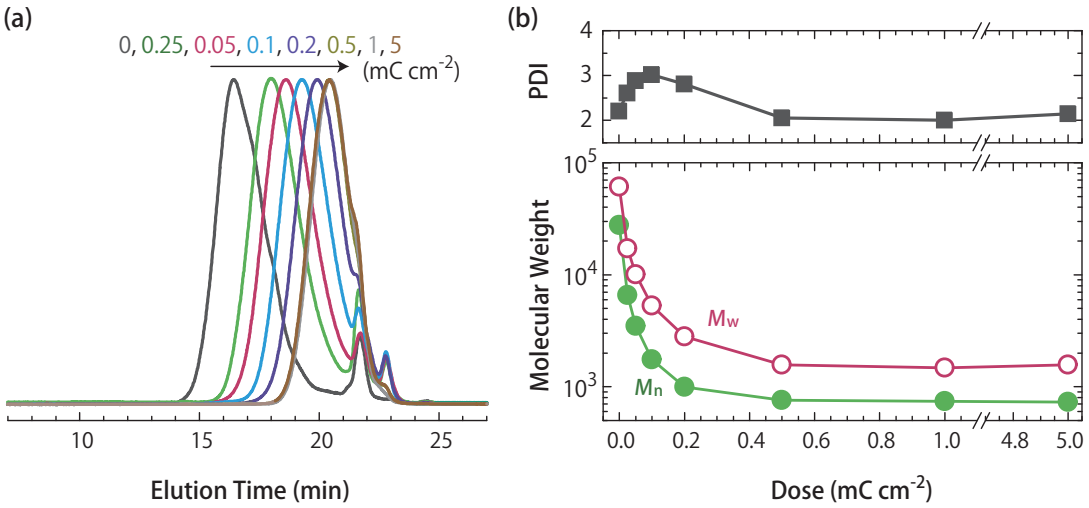

Fig. 2.3 | (a) GPC curves of blank and EB-irradiated ZEP520A and (b) calculated molecular weight and PDI.

2.3.2 Structural transitions

UV-vis spectroscopy

As shown in Fig. 2.4, the absorption bands of the irradiated ZEP520A shift to a longer wavelength with increasing irradiation dose as compared with the blank sample. In addition to the absorbance of unsaturated bonds at around 190–300 nm (C=C and C=O), absorbance at 300–400 nm starts to increase for doses higher than 5 mC cm^{-2}, which suggests the generation of conjugated double bonds.[44,45] The peaks around 217, 258, 296, and 335 nm can be assigned to dienes (–C=C–C=C–), trienes (–C=C–C=C–C=C–), tetraenes (–C=C–C=C–C=C–C=C–), and pentaenes (–C=C–C=C–C=C–C=C–C=C–), respectively.[44,45] Similar results were also obtained for ZEP7000.

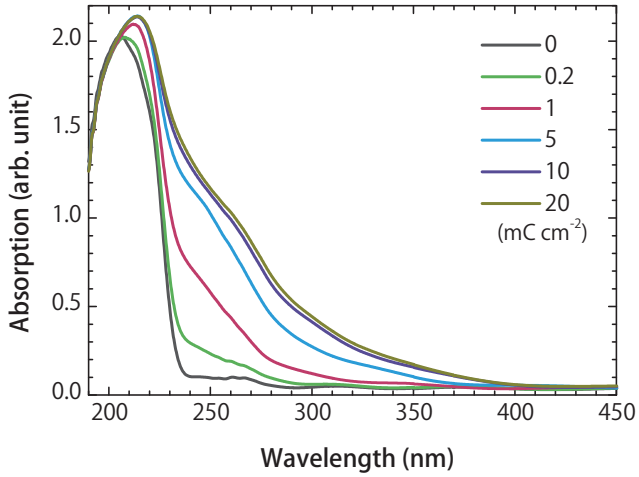

Fig. 2.4 | UV-vis spectra of ZEP520A for high-dose irradiation by 100 kV EB.

FT-IR spectroscopy

The FT-IR spectra changed drastically for the high-dose irradiated ZEP resists. The absorbance at around 1050–2050 cm^{-1} was decreased; this indicates that the ester side-chains were decomposed. Moreover, doublet peaks of C=O (1750 and 1725 cm^{-1}) and C–O (1240 and 1200 cm^{-1}) became singlet. This would suggest that chlorine atoms were consumed by the high-dose irradiation.

XPS

The ratios of O/C, Cl/C, and N/C in ZEP resists were evaluated by XPS and summarized in Table 2.1. As shown in the XPS spectra (Fig 2.6), Cl was completely eliminated at around 10 mC cm^{-2}.

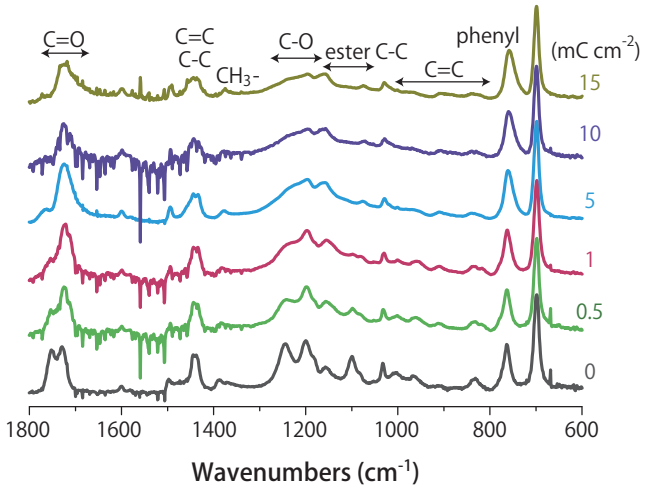

Fig. 2.5 | FT-IR spectra of ZEP520A for high-dose irradiation by 100 kV EB.

The intensities of O and N are increased by irradiation due to the formation of oxide and amine groups during the irradiation or after exposure to air. However, these factors would not influence P–N inversion because the O and N are saturated for doses higher than 1 mC cm^{-2}. Upon comparing these results with the sensitivity curves in Fig. 2.2, it is observed that the resists undergo P-N inversion as Cl is eliminated for irradiation doses higher than 10 mC cm^{-2}.

Table 2.1 | Ratios of O/C, Cl/C, and N/C of ZEP resists evaluated by XPS.

Dose (mC cm^{-2})	O/C		Cl/C		N/C	
	ZEP520A	ZEP7000	ZEP520A	ZEP7000	ZEP520A	ZEP7000
0[a)]	0.15	0.15	0.077	0.077	0	0
0[b)]	0.16	0.16	0.086	0.086	N.D.	N.D.
0.1	0.24	0.24	0.065	0.059	0.036	0.040
1	0.24	0.27	0.036	0.042	0.052	0.068
5	0.25	0.25	0.009	0.018	0.045	0.056
10	0.24	0.26	0.006	0.005	0.051	0.069
15	0.24	0.25	N.D.	N.D.	0.060	0.064
20	0.24	0.25	N.D.	N.D.	0.052	0.052

a) theoretical b) measured N.D. : not detected

The numbers of C–C bonds (284 eV, including C–H and C=C) and C–Cl bonds per monomer unit were evaluated by their relative ratios. As shown in Fig. 2.7, it was found that C–C bonds are partially recovered while the C–Cl bonds disappear. Nearly identical results were obtained with ZEP7000.

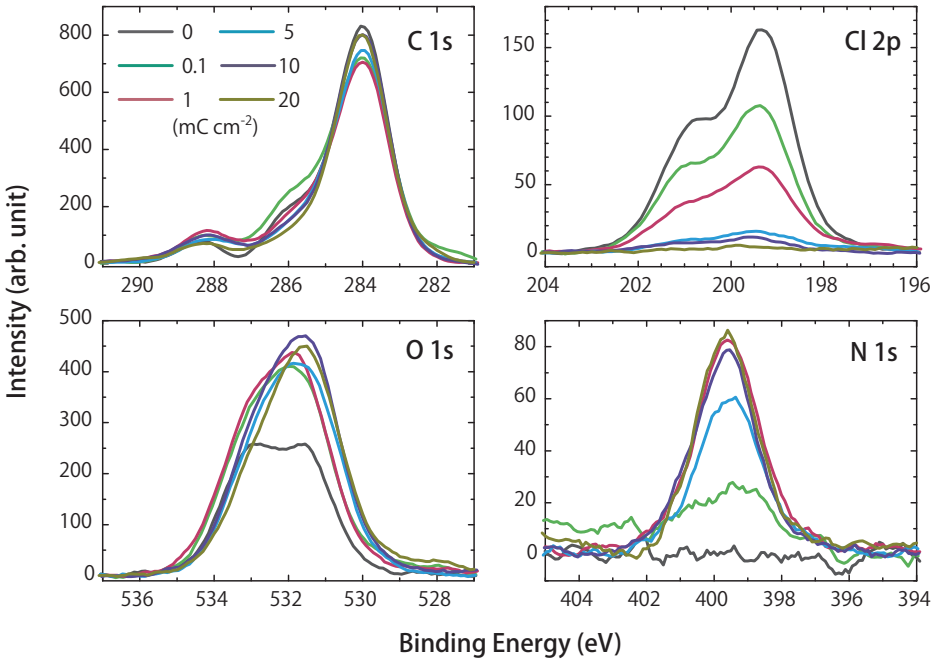

Fig. 2.6 | XPS spectra of ZEP520A for high-dose irradiation by 100 kV EB.

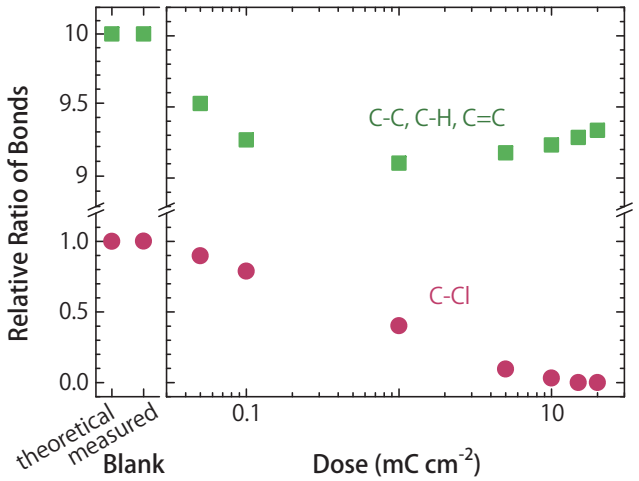

Fig. 2.7 | Relative ratios of C–C (C–H, C=C) and C–Cl bonds in ZEP520A.

NMR spectroscopy

The decrease in the number of the side-chains as suggested by FT-IR spectra (Fig 2.5) was also confirmed by the NMR spectra shown in Fig. 2.8. A noticeable decrease in α-methyl (0.6–1.7 ppm), ester (2.5–3.8 ppm), and phenyl groups (6.8–7.3

ppm) was observed for doses higher than 0.5 mC cm^{-2}. These side-chain cleavages would form conjugated double bonds in the main-chain, as observed in UV-vis spectra shown in Fig. 2.4.

Moreover, the terminal C=C double bonds generated via main-chain scission (4.8 –6.5 ppm) reduced in quantity for doses higher than 0.5 mC cm^{-2}. This indicates that the terminal double bonds were consumed due to the crosslinking reaction among the decomposed chains. The obtained result was consistent with the recovery of molecular weight observed with GPC curves shown in Fig. 2.3.

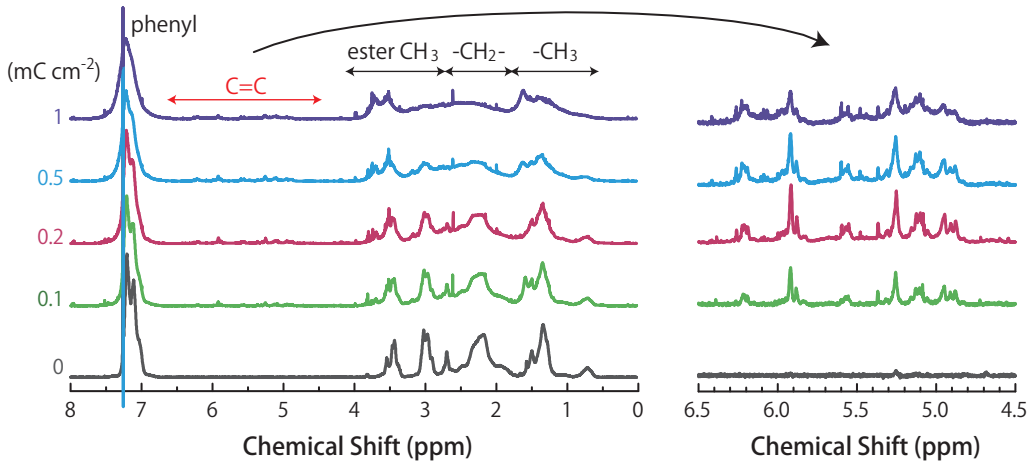

Fig. 2.8 | ^{1}H-NMR spectra of ZEP520A for high-dose irradiation by 100 kV EB.

2.4 Summary

Chapters 1 and 2 discussed the reaction mechanisms of main-chain scission and crosslinking in ZEP resists. P-N inversion was induced due to elimination of chlorine atoms from the resists for doses of around 10 mC cm^{-2}. The results suggest that the chlorine content in the ZEP resists plays an important role in the determination of the scission/crosslinking probabilities and the threshold of the P-N inversion.

The crosslinking in ZEP resists was confirmed by the reduction in the number of terminal double bonds that formed via main-chain scission. In addition, cleavages of side-chains generated conjugated double bonds in response to the irradiation dose. For high-dose irradiation, the structural changes and the lower scission rate due to the decreased chlorine amounts would change the positive-tone ZEP resists into negative-tone.

3

Linear Energy Transfer Effects on Resist Performance

In this chapter, we examine ZEP resists irradiated with 30 and 75 keV EBs and 6 MeV/u heavy ion beams (Si^{14+}, Ar^{18+}, Kr^{36+}, and Xe^{54+}). The sensitivities of the resists vary for these quantum beams, and the lower dose is required for the higher linear energy transfer (LET). However, the calculated absorbed dose becomes constant for low-LET EBs.

On the other hand, ZEP resists require more absorbed doses of high-LET ion beams in comparison with the doses of low-LET EBs. This would be due to the occurrence of high-density ionization events that degrade the efficiency of main-chain scission. In addition, the contiguous radicals may enhance probability of recombination or cross-linking. Moreover, the analysis suggests that the LET effects are dependent on the state of irradiated material, such as the molecular weight.

3.1 Introduction

Quantum beams deposit their energies as they pass through materials. Linear energy transfer (LET) is used as a measure of this type of energy deposition, which is dependent on radiation source and material. The LET is defined as the energy transferred per unit length, dE/dx, where dx denotes pass length and dE denotes the energy deposition through electronic collisions minus the kinetic energies of the secondary electrons. As schematically shown in Fig. 3.1, low-LET photons and EB form isolated spurs where the ionization event occurs. On the other hand, high-LET radiations like ion beams generate overlapped spurs in which dozens of ion pairs are included.

In this chapter, we examine ZEP resists irradiated by 30 and 75 keV EBs and 6 MeV/u heavy ion beams (Si^{14+}, Ar^{18+}, Kr^{36+}, and Xe^{54+}). From the obtained sensitivity curves, we discuss the dependence of resist performance on LET.

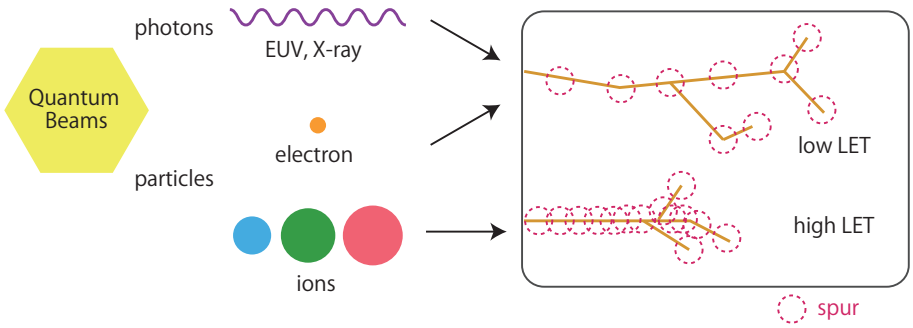

Fig. 3.1 | Schematic drawing of generated spurs for different values of LET.

3.2 Methods

Sample preparation of ZEP resists

Spin-coated ZEP samples were prepared as described in p. 16.

EB irradiation

Irradiation using 30 keV EB (JSM-6500F: JEOL) and 75 keV EB (ELS-7700: Elionix) were performed with a beam current of about 10 pA, under vacuum below 1×10^{-4} Pa. Square patterns with side lengths of 70 µm were irradiated to evaluate the dose-to-clear (E_0).

Ion beam irradiation

The experiments with the 6 MeV/u high energy ion beams, Si^{14+} (168 MeV), Ar^{18+} (240 MeV), Kr^{36+} (504 MeV) and Xe^{54+} (792 MeV), were carried out at the Medium Energy Experimental Port (MEXP) at Heavy Ion Medical Accelerator in Chiba (HIMAC) in National Institute of Radiological Science (NIRS).

The irradiation was performed at room temperature under vacuum ($<2\times10^{-4}$ Pa). The ion dose was estimated by the flux (about 1×10^{9} ions cm^{-2} $pulse^{-1}$) detected by a Faraday cup. The period of the beam pulse was 1.65 s and the dose was controlled by irradiation time and pulse duration. The elliptical beam size at the sample position was about 20×25 mm^2. Square Ni mesh masks with side lengths of about 70 μm were placed on the resist samples to facilitate pattern transfer, and to evaluate the dose-to-clear (E_0).

Measurements and simulations

The thicknesses of the spin-coated and developed resist samples were measured using an atomic force microscope (AFM, SPI3800: SII NanoTechnology). The energy deposition of the EBs and their trajectories were simulated using Monte Carlo simulation codes EGS5[27] and CASINO,[46–48] respectively. Those of the ion beams were simulated using SRIM/TRIM code.[49]

3.3 Results and Discussion

3.3.1 Resist sensitivities for electron beams

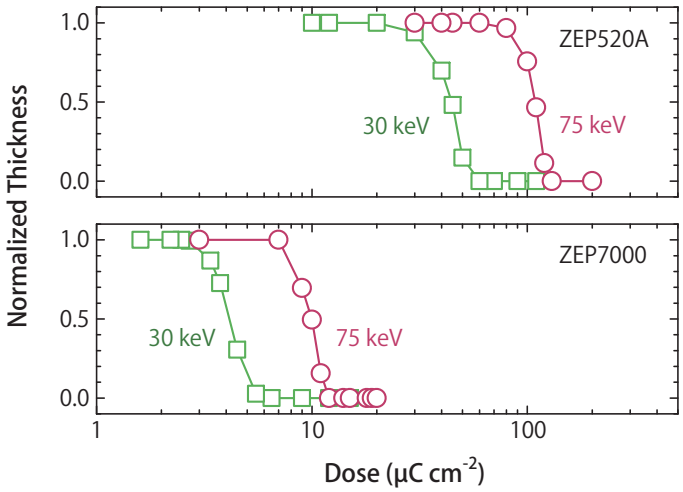

Fig. 3.2 | Sensivity curves of ZEP resists to 30 and 75 keV EBs.

The sensitivity curves obtained for EBs of 30 and 75 keV are shown in Fig. 3.2. The sensitivities (E_0) degrade with increasing EB energy: for EBs of 30 and 75 keV, the E_0 values of ZEP520A were 60 and 130 μC cm^{-2} and those of ZEP7000 were 5.8 and 12 μC cm^{-2}, respectively. On the other hand, the resist contrasts (γ) improved; as mentioned previously, this is defined as the tangent of the curve slope. For EBs of 30 and 75 keV, γ values of ZEP520A were 4.9 and 5.6, and those of ZEP7000 were 4.0 and 4.9, respectively.

The trajectories of EBs simulated by CASINO are shown in Fig. 3.3. The blue lines show the paths of primary electrons, and red lines show those of the backscattered electrons (BSE). A higher accelerating voltage significantly reduces the lateral spread of electrons in the resist. This fact shows the advantages of using thinner resist films and higher beam voltages for high resolution EB lithography. Moreover, a considerable number of BSE from the Si substrate irradiates the resist. Increasing the EB energy decreases the broadening of the BSE, thereby leading to improvement in the resolution.

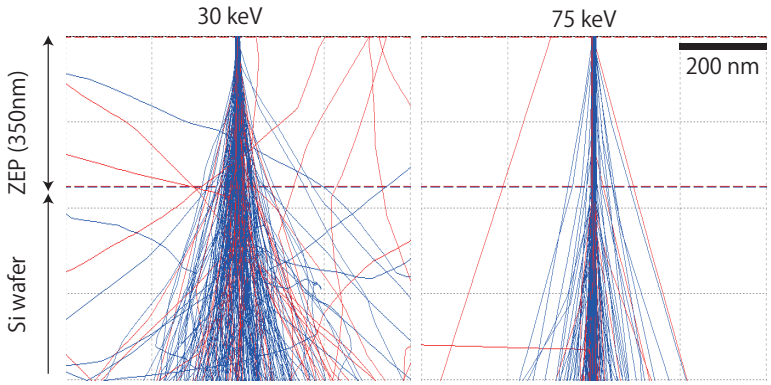

Fig. 3.3 | Simulated trajectories of EBs (ϕ =10 nm) in 350 nm-thick ZEP resist on Si wafers. (primary electrons: blue, BSEs: red)

The energy depositions of the EBs were calculated using EGS5.[27] The LETs of the 30 and 75 keV EBs were 1.48 and 0.706 eV nm^{-1}, respectively. It is considered that the higher LET of the 30 keV EB induced more main-chain scission in the resists, and subsequently, higher sensitivities were obtained. With respect to the BSE from the Si substrate, the deposited energy was increased by approximately 1.6 times, and this energy became equivalent to LETs of 2.43 and 1.08 eV nm^{-1} for the 30 and 75 keV EBs, respectively.

The absorbed dose (D_0) corresponding to the sensitivity (E_0) can be calculated by using the LET. Then, for the 30 and 75 keV EBs, the D_0 values of ZEP520A were 900 and 880 kGy, respectively, and those of ZEP7000 were 88 and 81 kGy, respectively. The values of D_0 were almost constant for these EBs.

3.3.2 Resist sensitivities for ion beams

Figure 3.4 shows the sensitivity curves for 6 MeV/u Si^{14+}, Ar^{18+}, Kr^{36+}, and Xe^{54+}. As summarized in Table 3.1, the sensitivities varied with the choice of irradiated ions. Higher sensitivities were obtained for increasing beam energy. Moreover, the resist contrasts (γ) were higher than those for the EBs.

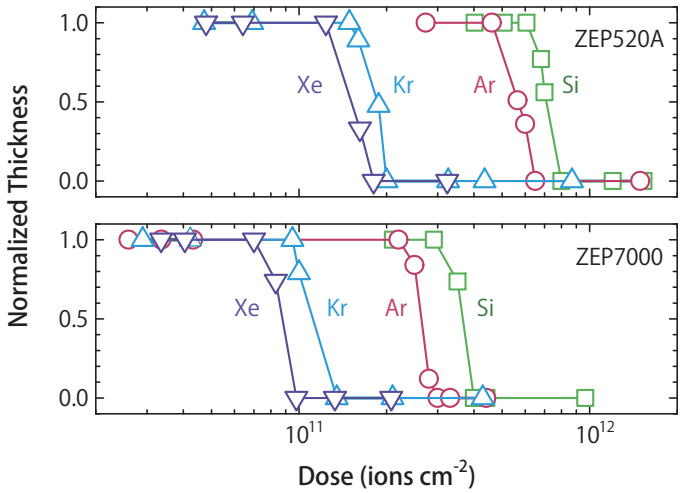

Fig. 3.4 | Sensitivity curves for ZEP resists upon irradiation by 6 MeV/u ion beams.

Table 3.1 | Sensitivities (E_0) and contrasts (γ) for the 6 MeV/u ion beams.

Resist	E_0 (ions cm^{-2}) [γ]			
	Si^{14+}	Ar^{18+}	Kr^{36+}	Xe^{54+}
ZEP520A	8.0×10^{11} [8.0]	6.5×10^{11} [6.7]	2.0×10^{11} [7.8]	1.8×10^{11} [6.1]
ZEP7000	4.0×10^{11} [7.3]	3.0×10^{11} [7.4]	1.4×10^{11} [6.6]	9.8×10^{11} [6.8]

The ion trajectories for 240 MeV Ar^{18+} simulated using the SRIM/TRIM code are shown in Fig. 3.5. The primary ions penetrate the ZEP and enter the Si wafer. The small lateral spread of the beam contributes to the high contrasts. Moreover, it is observed that the resulting reduction in BSE is one of the main advantages of ion beam lithography over EB lithography.

Figure 3.6 shows the stopping powers (which are synonymous with LET) of the irradiated ions. The stopping power changes in the material as a function of the penetration depth. Since the resist samples were very thin, the average energy deposition can be assumed to be equal to that at the sample surface. Consequently, the LETs of the Si^{14+}, Ar^{18+}, Kr^{36+}, and Xe^{54+} were calculated to be 1.6, 2.5, 7.4, and 13.3 keV nm^{-1}, respectively. These values are much larger than those obtained for the EBs.

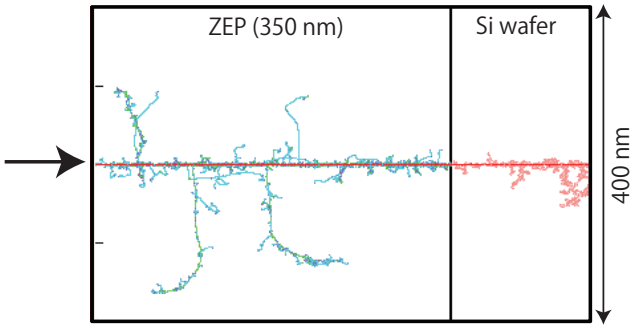

Fig. 3.5 | Ion trajectories of 240 MeV Ar^{18+} (red) in ZEP along with the recoils.

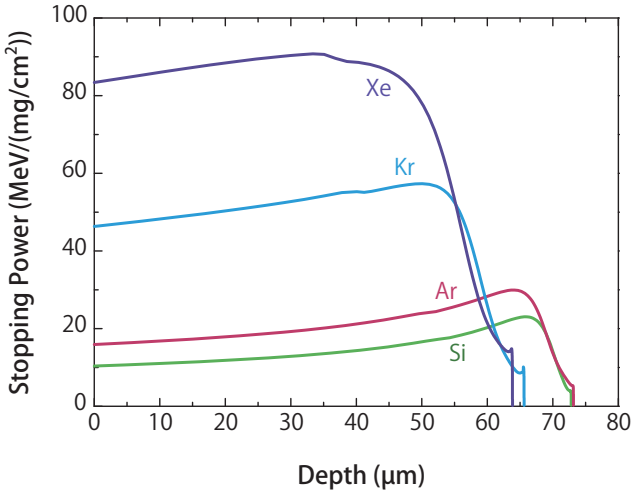

Fig. 3.6 | Stopping powers for 6 MeV/u Si^{14+}, Ar^{18+}, Kr^{36+} and Xe^{54+} in ZEP.

3.3.3 Linear energy transfer effects

The obtained sensitivities for the EBs and ion beams are summarized in Fig 3.7 (a), given in particles cm^{-2}. It is observed that the lower irradiation dose was required for the higher LET. However, as shown in Fig 3.7 (b), the calculated absorbed doses (given in MGy = 10^6 J kg^{-1}) reduced the sensitivity gap between the EBs and ion beams. The absorbed dose was identical for the two EBs. On the other hand, the required absorbed dose slightly increased for the ion beams, in response to the increase in LET. This would indicate that the resists became less sensitive to ion beams with higher values of LET. Moreover, the difference in sensitivity between ZEP520A and ZEP7000 was about 10 times for the EBs, but it reduced to about 2 times for the ion beams. ZEP7000 was more affected by the LET value than ZEP520A.

The reasons for the degraded sensitivities are speculated as follows. As shown in Fig. 3.8, high-LET ion beams induce ionization events in a limited space. Thus, the

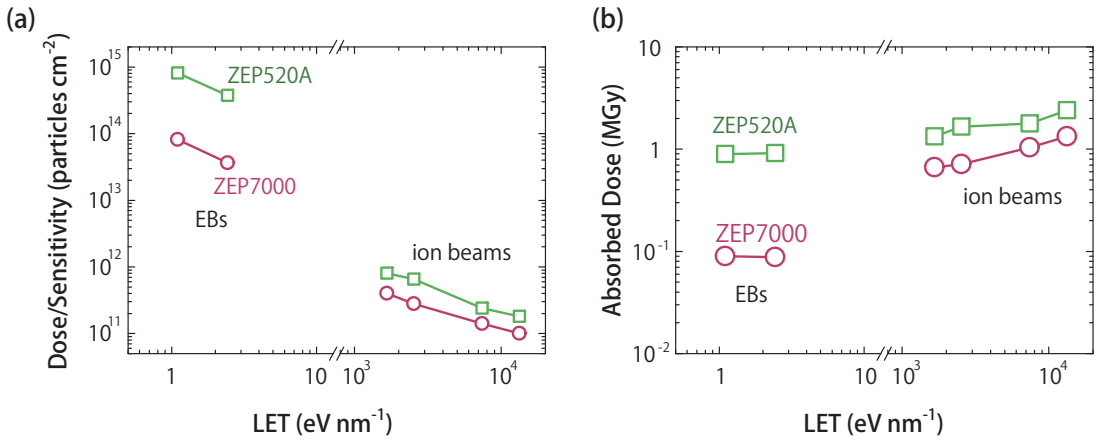

Fig. 3.7 | (a) Obtained sensitivities and (b) absorbed dose for the irradiated quantum beams with different LET values.

efficiency of the main-chain scission would be lower than that for low-LET beams. In addition, the contiguous radicals may enhance the probability of radical recombination or inter/intra-molecular crosslinking. The LET effects appeared prominently for ZEP7000 because of its high molecular weight. The detailed reaction mechanisms need to be discussed with respect to the heterogeneous energy distribution in the ion tracks.

It should be noted that the resists still dissolved in the developers without visible residues, and P-N inversion was not detected with the irradiated dose in this case. High-dose irradiation using these high-energy heavy ion beams was difficult because the samples become highly radioactivated.

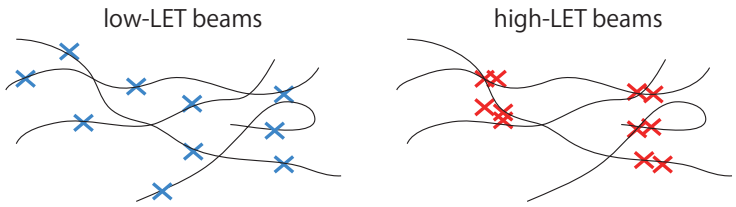

Fig. 3.8 | Ionization events in polymers induced by low- and high-LET beams.

3.4 Summary

In this chapter, we examined ZEP resists irradiated by low-LET EBs and high-LET ion beams. From the sensitivity curves and calculated absorbed doses, the dependence of resist performance on LET was discussed.

The sensitivities varied, and the lower dose was required for the higher LET. However, the calculated absorbed doses became constant for low-LET EBs. This result is applicable for other low-LET quantum beams such as EUV and X-rays; the relevant details are discussed in the next chapter. On the other hand, it was found that the resists required more absorbed doses of high-LET ion beams in comparison with low-LET EBs. The possible reasons for the degraded sensitivities would be the low probability of main-chain scission, radical recombination, and inter/intra-molecular crosslinking. In addition, LET effects appear to be dependent on the state of the irradiated material, such as its molecular weight.

This study focused on LET, and the induced reactions were discussed using a macroscopic approach. However, the detailed reaction mechanisms require to be discussed with respect to the microscopically heterogeneous energy distribution in the ion tracks.

4

Absorption Properties and Resist Performance

Extreme ultraviolet (EUV) and soft X-rays are considered as promising exposure sources for mass-production of electronic devices for the 22 nm node and below. In this chapter, we evaluate the sensitivities of ZEP resists and PMMA irradiated with monochromated EUV/soft X-rays from synchrotron light.

The sensitivities vary with the exposure wavelength, and it is experimentally confirmed that the absorption property of the resists has a strong influence on the sensitivity. However, the absorbed dose (given in $\mathrm{Gy} = \mathrm{J\,kg^{-1}}$), calculated from the obtained dose/sensitivity and the respective linear absorption coefficient, is nearly independent of the wavelength, and each resist showed a specific constant value. Similar results were obtained for PMMA, which is also a main-chain scission type resist.

4.1 Introduction

As previously described, EUV is considered as the ultimate exposure source in projection lithography for mass-production of electronic devices. The wavelength of EUV for the 22 nm node and below is currently expected to be 13.5 nm. The reaction mechanisms induced by EUV/soft X-ray exposure are analogous to those of other ionizing sources such as EB and X-rays.[11,13,50] Consequently, the absorption of incident radiation in a resist is an important factor to determine the sensitivity, since the yield of main-chain scission would be dominated by the generated secondary electrons.[51–53]

This chapter discusses the effect of absorption properties on resist performance. The sensitivities of ZEP resists and PMMA were investigated for EUV/soft X-ray wavelengths down to 3.1 nm. Monochromated EUV/soft X-rays from synchrotron light were used for the exposure, and the dependence of the exposure wavelength on resist sensitivity was evaluated.

4.2 Methods

ZEP resists and PMMA with the M_w of 350,000 (Aldrich) were prepared as follows. All the processes were performed under ambient conditions at 25 °C. Espacer®300 (Showa Denko K. K.), which is an antistatic agent, was coated on all the resist samples at 2000 rpm for 60 s after the pre-bake. The thickness was less than 20 nm.

Sample preparation of ZEP resists

- Dilution:
  ZEP520A: ZEP-A (anisole, ZEON) =1:2
  ZEP7000: ZEP-D (diethylene glycol dimethyl ether, ZEON) = 2:1
- Wafer preparation: dehydration treatment at 180 °C, 10 min
- Spin-coating: 4000 rpm for 120 s, on the Si wafers
- Pre-bake: 180 °C, 180 s
- Development:
  ZEP520A: ZED-N50 (n-amyl acetate 100%), 60 s
  ZEP7000: ZED-500 (3-pentanone 50%, diethyl malonate 50%), 60 s
- Rinse:
  ZEP520A: ZMD-B (methyl isobutyl ketone 89%, isopropyl alcohol 11%), 10 s
  ZEP7000: ZMD-D (methyl isobutyl ketone >99%),10 s

The thicknesses of both ZEP520A and ZEP7000 films after the pre-bake were approximately 80 nm.

Sample preparation of PMMA

- Dissolution: 0.7 g in 25 cc Toluene (Kishida Chemical, 99.5%)
- Wafer preparation:
  HMDS* (ROHM and HASSHMDS) was coated on Si wafers at 3000 rpm for 60 s and baked at 180 °C for 10 min
- Spin-coating: 2500 rpm for 120 s, on the HMDS-coated Si wafers
- Pre-bake: 220 °C for 15 min
- Development: MIBK (Wako):IPA (Kanto Chemical)= 1:3 for 60 s

The thickness of the PMMA after the pre-bake was approximately 260 nm.

EUV/soft X-ray irradiation

Monochromated EUV/soft X-rays from the BL27SU of the SPring-8 were used for the exposure.[54] The SPring-8 is the world's largest synchrotron radiation facility with an 8 GeV storage ring and a stored current of 100 mA. The X-ray wavelengths used in the experiment were 3.1, 3.9, and 5.0 nm (400, 320, and 250 eV). The selected flux was approximately 2×11^{10} photons s^{-1} mm^{-2} with the energy spread ($E/\Delta E$) being approximately 50,000. The irradiated dose was obtained by integrating the flux, which was evaluated with a photodiode (AXUV), and its quantum efficiency to each wavelength. The samples were irradiated under vacuum below 1×10^{-4} Pa. The beam size was approximately 0.2 mm × 0.3 mm square at the sample position.

Measurements and simulations

The thicknesses of the spin-coated and developed resist samples were measured using an atomic force microscope (AFM, SPI3800: SII NanoTechnology). The linear absorption coefficients of the resists were calculated from the NIST Standard Reference Database 126.[55]

4.3 Results and Discussion

4.3.1 Sensitivities for EUV/soft X-rays

The sensitivity curves for the ZEP resists and PMMA are shown in Fig. 4.1. The sensitivities (E_0) and contrasts (γ) are summarized in Table 4.1. ZEP520A requires approximately 10 times more dose than ZEP7000, and this difference in sensitivity is the same as that for EB irradiation (shown in p. 37). The PMMA exhibited much lower sensitivities than ZEP resists.

*hexamethyldisilazane

It is noteworthy that the sensitivities varied with different exposure wavelengths. All the resists showed the highest sensitivities to 3.9 nm, and the lowest to 5.0 nm. In addition, the contrasts also correlated with the wavelength, even though the contrasts of ZEP7000 may contain some errors, because the lower doses could not be irradiated in this experiment due to the high flux of the BL27SU.

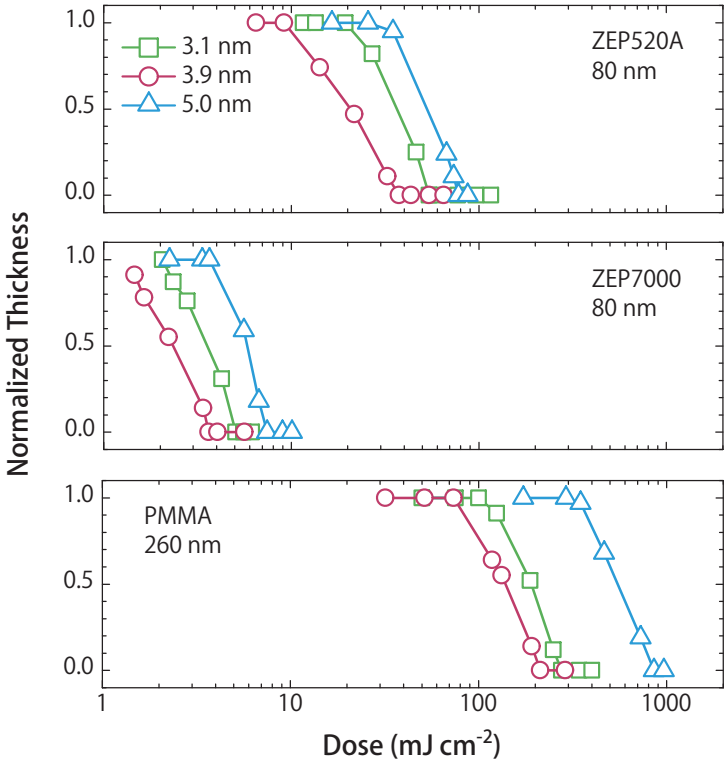

Fig. 4.1 | Sensitivity curves of ZEP resists and PMMA for EUV/soft X-rays.

Table 4.1 | Sensitivities (E_0) and contrasts (γ) for EUV/soft X-rays.

Resist	E_0 (mJ cm^{-2}) [γ]		
	3.1 nm	3.9 nm	5.0 nm
ZEP520A	54 [2.2]	38 [1.6]	78 [2.9]
ZEP7000	5.1 [2.8]	3.6 [1.9]	7.4 [3.3]
PMMA	276 [2.3]	214 [2.2]	858 [2.6]

4.3.2 Absorbed dose for sensitivity

In this section, the absorption properties of the resists are discussed. Figure 4.2 shows the absorption coefficients of ZEP and PMMA calculated using the NIST Data-

base,[55] assuming that their densities are 1.6 and 1.2 g cm^{-3}, respectively. According to the obtained sensitivities and contrasts, the resists exhibited higher sensitivities and lower contrasts for the wavelengths at which the resists have higher absorption coefficients.

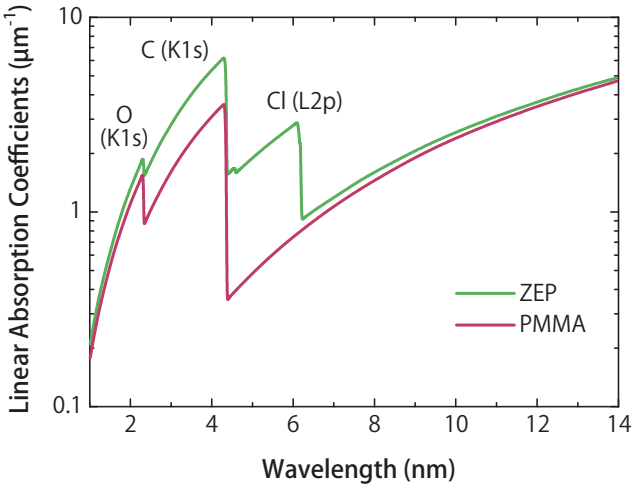

Fig. 4.2 | Calculated linear absorption coefficients of ZEP and PMMA.[55]

The absorbed dose (D) in a resist is expressed as

$$D(T) = \alpha E_0 exp(-\alpha T) \tag{4.1}$$

where α denotes the linear absorption coefficient and T denotes the resist thickness. With the obtained dose/sensitivity (E_0, in mJ cm^{-2}) and calculated linear absorption coefficients, the absorbed doses in ZEP resists for each exposure wavelength were calculated, and expressed in terms of Gy (Gy = J kg^{-1}).

The absorbed doses decay exponentially with resist thickness. However, the absorbed doses at the bottom of the resists (D_0) which corresponds to E_0, were almost constant for each resist, regardless of the exposure wavelength (ZEP520A: ~810 kGy, ZEP7000: ~77 kGy, and PMMA: ~2.5 MGy). The D_0 values of ZEP resists and PMMA were comparable to those for EB irradiation (ZEP520A: ~890 kGy, ZEP7000: ~85 kGy[†], PMMA: ~3.0 MGy[‡]). The reactions caused by EUV/soft X-rays would be identical to those caused by EB irradiation, except for the energy absorption processes.

Moreover, the contrast also correlated with the absorption property; the contrast value reduces with increased absorption. This can be accounted for by the energy deposition exponential curve shown in Fig. 4.3. With increased absorption, the absorbed dose significantly decreases with increasing depth. For practical use

[†] as mentioned in Chap. 3

[‡] E_0 for a 30 keV EB was approximately 300 μC cm^{-2}.

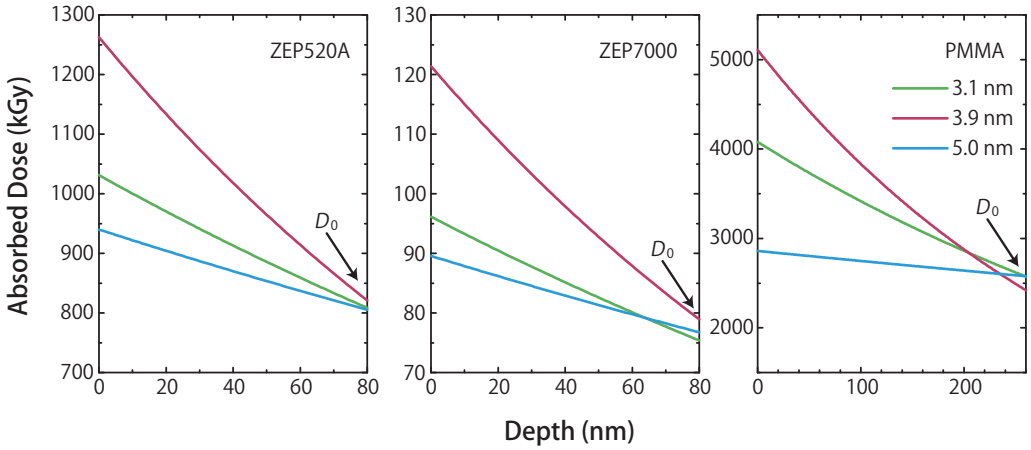

Fig. 4.3 | Calculated absorbed dose in ZEP resists and PMMA.

for EUV/soft X-ray lithography, the resist thickness should be reduced to avoid this contrast degradation, which is caused by the absorption difference along the depth direction.

4.4 Summary

The resist sensitivities of ZEP resists and PMMA for monochromated EUV/soft X-rays were evaluated. The sensitivities varied with the exposure wavelength, and it was experimentally confirmed that the absorption property has a strong influence on the sensitivity. However, it was confirmed that the absorbed dose, calculated from the dose/sensitivity and the corresponding linear absorption coefficients, was nearly independent of the wavelength. Similar results were also obtained for PHS-based CA resists.[56)]

Chapters 3 and 4 discuss the resist sensitivities in terms of absorbed dose. For the EBs and EUV/soft X-rays with low LET, each resist has a particular value of required absorbed dose, regardless of the irradiation source. The reactions caused by EUV/soft X-rays would be identical to those by EB, except for the energy absorption processes. On the basis of this result, once the resist sensitivities for a certain wavelength (or an EB) are experimentally obtained, those for other exposure wavelengths can be estimated. The predictions of resist sensitivity are demonstrated in Chap. 2 of Part II.

Part II

Applications to Advanced Technologies

1

Micro/Nanofabrication Technique Using Positive-Negative Inversion

This chapter reports a unique fabrication technique that utilizes the positive-negative (P-N) inversion of ZEP resists (described in Chap. 2 of Part I).

By controlling the P-N inversion in combination with the three-dimensional energy deposition distribution of the irradiated quantum beam, it could be ensured that the resist in the beam spot locally became negative-tone, while in the surrounding area and near the edge of the beam penetration range, the resist remained as positive-tone. Consequently, only the crosslinked regions are peeled off from the bulk resist, as "nanobead from nanocup". Desired micro/nanostructures such as sub-millimeter-length wires and nanomembranes can be successfully obtained using a focused ion beam.

1.1 Introduction

Along with miniaturization techniques for higher integration, novel fabrication techniques have attracted considerable attention recently because of the increasing and diversified demands for various electronic devices, bio and medical components, optical devices, and so on.

This chapter reports a unique micro/nanofabrication technique that utilizes the P-N inversion of ZEP resists. As described in Chap. 2 of Part I, ZEP resists undergo P-N inversion by high-dose irradiation of EB. By controlling the P-N inversion in combination with the three-dimensional energy deposition distribution of the irradiated quantum beam, it could be ensured that the resist in the beam spot locally changes to negative-tone, while it remains positive-tone in the surrounding area of the beam spot and near the edge of the penetration range of the beam. In this chapter, we discuss ZEP resists irradiated with a 30 keV Ga^+ focused ion beam (FIB) in attempting the abovementioned novel fabrication technique.

1.2 Methods

Sample preparation of ZEP resists

Spin-coated samples were prepared by the standard procedure described in p. 16.

FIB irradiation

Ga^+ ion irradiation was carried out using a 30 keV FIB (SMI2050, SII NanoTechnology) with a beam current of 9 pA under 1×10^{-4} Pa at 25 °C.

Measurements and simulations

The sample surfaces were observed using an AFM (SPI3800: SII NanoTechnology) and a digital microscope (VHX-1000: KEYENCE). Simulations of the ion penetration range and energy deposition were performed as described in p. 37.

1.3 Results and Discussion

1.3.1 Positive-negative inversion induced by ion beam

After the Ga^+ FIB irradiation, the resist thicknesses of the irradiated areas were found to have decreased slightly even without the development processes. The resists appeared to be directly etched by Ga^+ ions. As shown in Fig. 1.1 (a), the etching

rates of the ZEP resists were almost identical. This could be attributed to the fact that both resists are composed of the same copolymer.

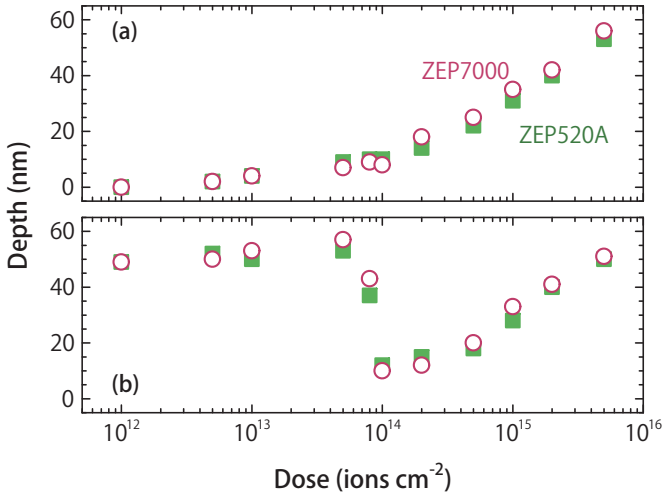

Fig. 1.1 | Fabricated depths of 30 keV Ga^+-irradiated ZEP resists (a) before and (b) after development.

Subsequently, these samples were developed, and the fabricated depths were measured again with the AFM (Fig. 1.1 (b)). For an irradiation dose of 1×10^{12} ions cm^{-2}, the obtained depths were approximately 50 nm. Considering that the etching depths for the same dose were almost zero as shown in Fig. 1.1 (a), it can be concluded that the electronic effect of the FIB irradiation induced the main-chain scission and that the resists dissolved in the developers to a depth of 50 nm. Similarly, the fabricated depths were almost uniformly 50 nm for each dose up to 5×10^{13} ions cm^{-2}, after subtracting the respective etching depths. The depth of 50 nm was consistent with the theoretically simulated ionizing energy deposition range of Ga^+ ions into ZEP resists, as shown in Fig. 1.2. Further, it was found that the doses required for the resists to be dissolved in the developers were less than 1×10^{12} ions cm^{-2}.

In contrast, for doses higher than 5×10^{13} ions cm^{-2}, the fabricated depths were almost the same as the etching depths. These results indicate that the resists underwent P-N inversion due to the reason described in Chap. 2 of Part I. In addition, it was found that the P-N inversion is independent of the molecular weight.

1.3.2 Linear energy transfer effects

As mentioned in Chap. 2 of Part I, ZEP resists undergo P-N inversion with a 100 kV EB when the dose is higher than 10 mC cm^{-2}, *i.e.*, approximately 6.25×10^{16} electrons cm^{-2}. On the other hand, the Ga^+ ions induced P-N inversion with only 5×10^{13} ions cm^{-2}. This is attributable to the difference in the LET.

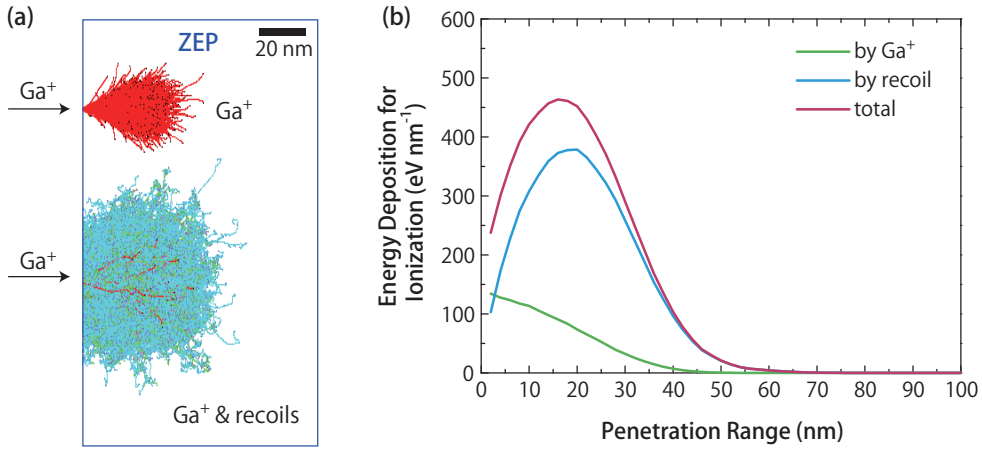

Fig. 1.2 | (a) Simulated trajectories of 30 keV Ga^+ and the recoils in ZEP, and (b) energy deposition.

The LET calculated using EGS5 for the 100 kV EB in ZEP resists was approximately 1 eV nm^{-1}, in consideration of the BSEs from the Si wafer. The LET for 30 keV Ga^+ ions was calculated as shown in Fig. 1.2 (b). The deposited energies of both the 100 kV EB and the 30 keV Ga^+ were calculated by integrating respective LETs from the surface to a depth of 50 nm (100 kV EB: 50 eV, 30 kV Ga+: 13.6 keV). Subsequently, the total absorbed dose (deposited energy × irradiated dose) for the threshold of the P-N inversion was obtained. The total absorbed dose for 100 kV EB was 4.5 times that for 30 kV Ga^+.

In the case of ion-beam-irradiated PMMA, LET is reported to have a significant effect on the P-N inversion, which shows that a high LET caused by ion-beam irradiation drastically reduced the dose window between sensitivity (as positive-tone) and the threshold of P-N inversion.[43] In contrast, the obtained results revealed that the LET effects on ZEP were smaller than that of PMMA, and a wide dose-window was observed between the sensitivity ($<1\times10^{12}$ ions cm^{-2}) and the P-N inversion (5×10^{13} ions cm^{-2}).

1.3.3 Novel fabrication method—nanobead from nanocup technique

By applying the results regarding P-N inversion in combination with the three-dimensional energy distribution of the ion beam, a unique fabrication technique of micro/nanostructures was developed.

The intensity of the FIB was assumed to have a Gaussian distribution. Although most of the ions were deposited in the central part of the beam (beam spot), low-density ions (halo-beam) and recoils were distributed in the outer and surrounding areas of the beam spot. Thus, by choosing an appropriate irradiation dose, it can be

ensured that the resists at the center of the beam spots locally change to negative-tone (crosslinking). The resists in the surrounding area of the beam spots reacted as positive-tone (main-chain scission) and dissolved in the developers. Further, the reaction of resists was considered to be a main-chain scission near the edge of the penetration range of Ga^+ ions because of the low-energy deposition, as shown in Fig. 1.2. Hence, it was expected that only the crosslinked regions would be peeled off from the irradiated areas in the developers.

Figure 1.3(a) shows the scheme of "nanobead from nanocup". In the developer (developed for 75 s), nanobeads successfully peeled off from nanocups of the bulk resist, as shown in the AFM images in Fig. 1.3(b). The average thickness of the obtained nanobeads was approximately 50 nm, and this thickness reflects the penetration range of the ions.

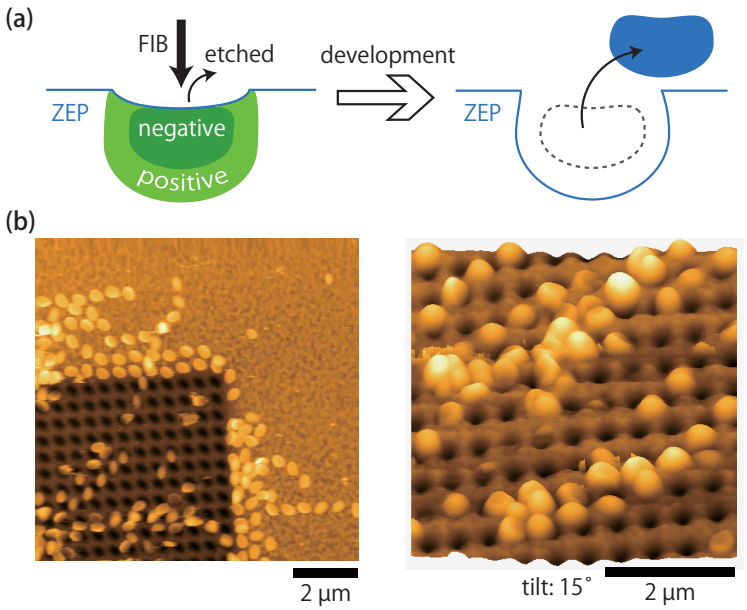

Fig. 1.3 | (a) Schematic drawing of "nanobead from nanocup" and (b) AFM images of nanobead peeled from nanocup (dose: 5×10^{14} ions cm^{-2}).

The desired micro/nanostructures can be fabricated by extending the "nanobead from nanocup" to higher dimensions. Figure 1.4 shows the membrane, beads, and wires obtained by irradiation of ZEP7000 using a dose of 1×14^{16} ions cm^{-2}, after development for 75 s.

A thin membrane could be lifted off from the bulk resist, which was irradiated over an area of 50 μm square. For narrow pitch irradiation, the beam spots overlap each other; in such cases, the entire irradiated area was considered to become negative-tone. Subsequently, a membrane with a nanoscale thickness could be obtained after development. The thickness of the membrane was approximately 60 nm,

and this reflects the penetration range of the ions. In contrast, when beam spots are completely isolated, nanobeads were obtained. Furthermore, by selecting an appropriate beam pitch, nanowires on the plain axis were fabricated. It was interesting to observe that the obtained wires were shaped like beads on a string. The sizes of the obtained beads and wires as defined in Fig. 1.4 were (d, h) = (500 nm, 60 nm) and (w, h, l) = (400 nm, 60 nm, 6 μm). The values of d, w, and l could be controlled by tuning irradiation conditions such as beam size and scanning length. Sub-millimeter-length wires were obtained as shown in Fig. 1.5, with the dimensions of (w, h, l) = (900 nm, 60 nm, 800 μm).

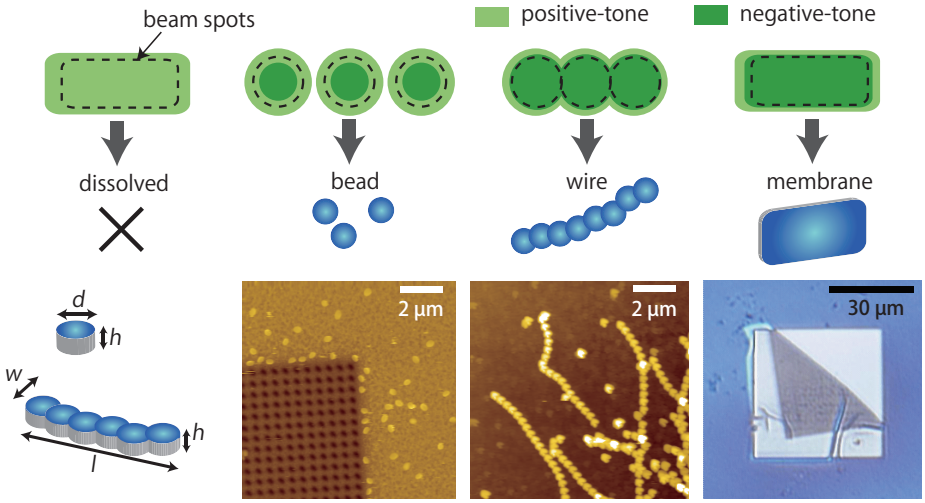

Fig. 1.4 | Irradiated areas peeled off as beads, wires (AFM images), and membrane (optical microscope image).

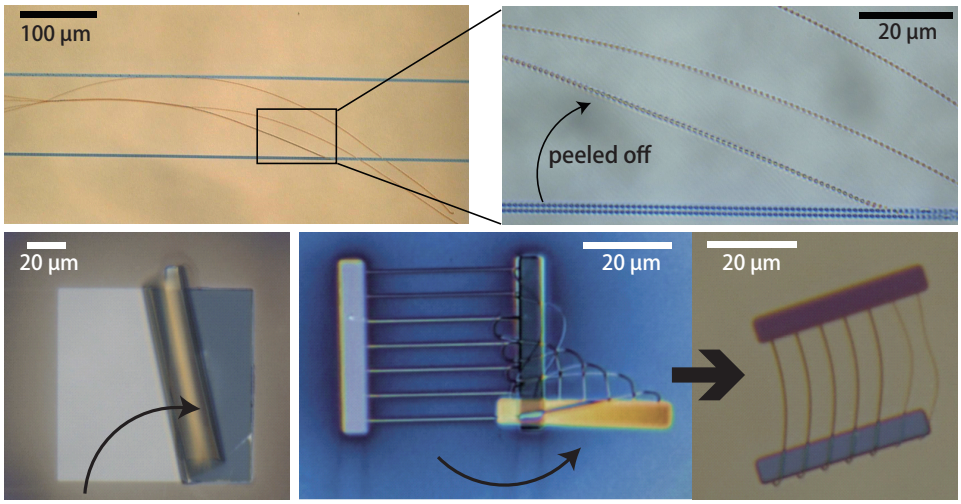

Fig. 1.5 | Obtained mico/nanostructures.

1.4 Summary

By controlling the P-N inversion of ZEP resists in combination with the three-dimensional energy deposition distribution of the irradiated quantum beam, a novel micro/nanofabrication technique was demonstrated. The technique is applicable to other ion beams, and the thickness of the micro/nanostructures can be controlled by their penetration ranges. For example, 10 keV Ga^+ and 50 keV Ar^+ will realize approximately 30 nm-thick and 100 nm-thick nanobeads, respectively. The isolated micro/nanostructures realized by using the "nanobead from nanocup" technique can have several potential applications, such as in optical devices and chemical/biomedical sensors.

An upcoming challenge is precise control of the feature size. It should be noted that the sizes of the obtained structures in this study were approximately 10% larger than the peeled areas. This increase in size would be attributed to the swelling of the crosslinked regions in the developer.

2

Evaluation of Resist Performance for Next-Generation Lithography

Extreme ultraviolet (EUV) lithography at a 13.5 nm exposure wavelength is soon to be introduced in high-volume manufacturing lines in 2013/2014,[5)] at and below the 22 nm node. Meanwhile, the potential application of wavelengths shorter than 13.5 nm for even higher resolutions has been discussed recently, particularly in the 6.x nm range (6.6–6.8 nm).

As described in Chap. 4 of Part I, it is observed that each resist has a particular value of required absorbed dose regardless of the irradiation source. On the basis of this result, resist sensitivities at 6.x nm exposure wavelengths are predicted in this chapter. Resists containing sulfur and/or silicon are considered promising candidates for use as high sensitivity resists in 6.x nm EUV lithography.

The sensitivities of ZEP resists, poly(methyl methacrylate) (PMMA), and hydrogen silsesquioxane (HSQ) are actually measured using a 6.7 nm EUV source, and it is confirmed that the obtained sensitivities are consistent with the predicted ones. The predictions of resist sensitivity demonstrated here will be very useful for the selection or development of resists for next-generation EUV lithography.

2.1 Introduction

As described in the introduction of this dissertation (p. 3), the semiconductor industry has repeatedly moved toward shorter wavelength exposure tools in order to achieve higher resolutions. Extreme ultraviolet (EUV) lithography at a 13.5 nm exposure wavelength is being considered as the most promising projection lithography at and below the 22 nm node. This technique is soon to be introduced into pilot lines in 2011, replacing ArF immersion lithography, and high-volume manufacturing is expected to begin in 2013/2014.[5)]

Meanwhile, the potential application of wavelengths shorter than 13.5 nm for even higher resolutions has been discussed recently. The development of proper optics is one of the primary challenges in the achievement of this goal. For example, an exposure wavelength of 6.x nm (6.6–6.8 nm) has been proposed as one of the primary candidates with reflective multilayer optics combinations of La/B_4C or C/B_4C, which offers a high reflectivity of over 70% for wavelengths around 6.7 nm.[57)] By shortening the exposure wavelength to 6.x nm, optical images with higher resolution can be obtained, and it would be possible to miniaturize feature sizes to below 11 nm, and possibly down to sub-5 nm level.[58–60)] Moreover, there are supportive estimations that the throughput with source power and system transmission efficiency for 6.x nm is comparable with that of 13.5 nm.[59,60)] Hence, exposure wavelengths in the EUV/soft X-ray region, especially 6.x nm, are expected to form the next-generation of EUV lithography.

However, these estimations have not included the resist performance, which is one of the most important criteria for practical lithography systems. A high sensitivity is required because the exposure light intensity and the resist sensitivity are complementary. Hence, this chapter focuses on evaluation of resist performance for next-generation EUV/soft X-ray lithography, especially at 6.x nm.

2.2 Methods

Sample preparation

ZEP520A, ZEP7000, and PMMA (M_w = 350,000, Aldrich) were prepared and developed as described in p. 44. Hydrogen silsesquioxane (HSQ) 6% solution in MIBK (DOW CORNING, XR-1541-006) was prepared as follows.

- Wafer preparation:
  HMDS* (ROHM and HASSHMDS) was coated on Si wafers at 3000 rpm for 60 s

*hexamethyldisilazane

and baked at 180 °C for 10 min
- Spin-coating: 3000 rpm for 60 s, on the HMDS-coated Si wafers
- Pre-bake: 150°C, 120 s followed by 220°C, 120 s
- Development: NMD-3 2.38% (TMAH[†]: Tokyo Ohka Kogyo), 60 s
- Rinse: deionized water, 15 s

The thickness after the pre-bake was approximately 160 nm. Espacer 300 (Showa Denko K. K.) was coated on the HSQ as described in p. 44.

EUV/soft X-ray irradiation, measurements, and simulations

The EUV/soft X-ray irradiation, measurements, and simulations were all conducted as described in Chap. 4 (p. 45).

2.3 Results and discussion

2.3.1 Prediction of resist sensitivities for 6.x nm EUV

In Chap. 4 of Part I, doses/sensitivities of typical resists were obtained in the EUV/soft X-ray region, and they were found to strongly depend on the wavelength. However, it was confirmed that the absorbed dose at the bottom of the resists (D_0), calculated from the dose/sensitivity (E_0) and the respective linear absorption coefficient (α), is almost independent of the wavelength, and this absorbed dose is constant for each resist; the expression for this absorbed dose is given as

$$D_0 = \alpha E_0 exp(-\alpha T_0) = \text{const.} \tag{2.1}$$

where T_0 denotes the resist thickness. On the basis of this result, once the resist sensitivities for a certain wavelength are experimentally obtained, those for other exposure wavelengths can be estimated. This consideration is applicable to the prediction of resist sensitivities for next-generation 6.x nm EUV lithography.

The sensitivities of ZEP resists and PMMA to 13.5 nm and 6.7 nm EUV were predicted by using the experimentally obtained D_0 values (p. 47) and the calculated linear absorption coefficients shown in Fig. 4.2. As summarized in Table 2.1, the sensitivities to the 13.5 nm EUV were expected to be equivalent to 3.9 nm. However, the sensitivity to 6.x nm wavelengths would be much lower, because the absorption coefficients are about a quarter of those for the 13.5 and 3.9 nm exposures.

Thus, resists containing certain high absorption elements around 6.x nm should be considered. Figure 2.1 shows the mass absorption coefficients at the 13.5 and 6.7

[†] tetra-methyl ammonium hydroxide

nm wavelengths; it can be deduced that resists containing sulfur ($Z = 14$) and/or silicon ($Z = 16$) are promising candidates. On the other hand, fluorine ($Z = 9$) which is suitable for 13.5 nm[53] would not contribute to high sensitivity for 6.x nm lithography. There are some commercially available resists containing sulfur and silicon.

Table 2.1 | Obtained and predicted sensitivities of ZEP resists to EUV/soft X-rays.

Resist	E_0 (mJ cm^{-2})				
	3.1 nm	3.9 nm	5.0 nm	6.7 nm	13.5 nm
ZEP520A (D_0 = 810 kGy)	54	38	78	**130***	**45***
ZEP7000 (D_0 = 77 kGy)	5.1	3.6	7.4	**12***	**3.8***
PMMA (D_0 = 2.5 MGy)	276	214	858	**470***	**270***

*predicted values

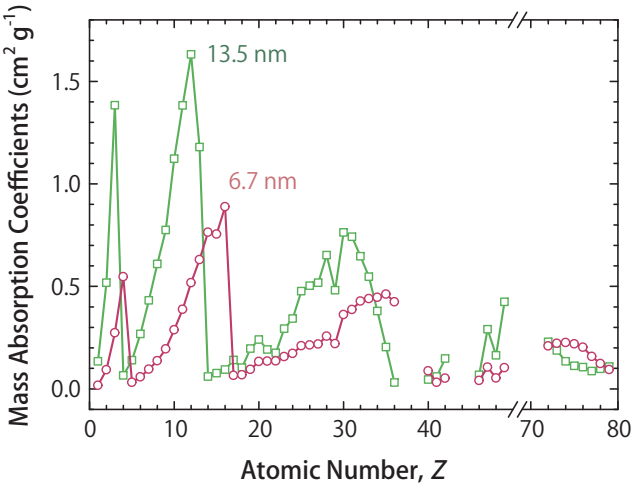

Fig. 2.1 | Mass absorption coefficients at 13.5 nm and 6.7 nm wavelengths.

Figure 2.2 shows the structures of hydrogen silsesquioxane (HSQ, 1.4 g cm^{-3}), poly(phenylsilsesquioxane) (PSQ, 1.56 g cm^{-3}), poly(2-methyl-1-pentenesulfone) (P-MPS, 2.2 g cm^{-3}). The linear absorption coefficients for these candidate resists were calculated as shown in Fig. 2.3. This clearly shows that the presence of silicon and sulfur increases the absorption of these resists significantly in the EUV/soft X-ray range in comparison with poly(hydroxy styrene) (PHS), which is the base polymer of chemically amplified (CA) resists that have been extensively studied for use in 13.5 nm EUV lithography. The absorption coefficients of ZEP, PMMA, PHS, and the resists containing sulfur/silicon are summarized in Table 2.2.

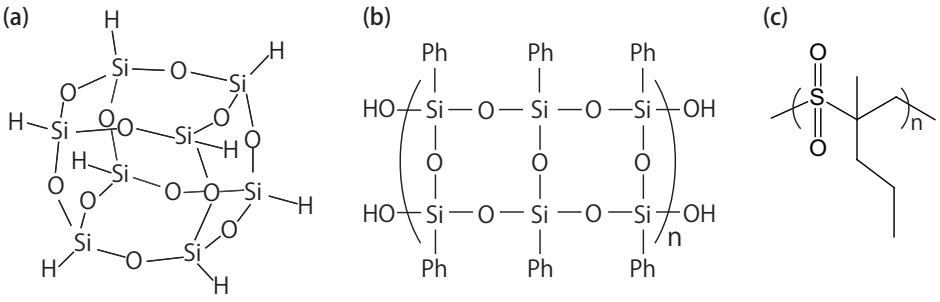

Fig. 2.2 | Structures of (a) hydrogen silsesquioxane (HSQ), (b) poly(phenylsilsesquioxane) (PSQ), and (c) poly(2-methyl-1-pentenesulfone) (PMPS).

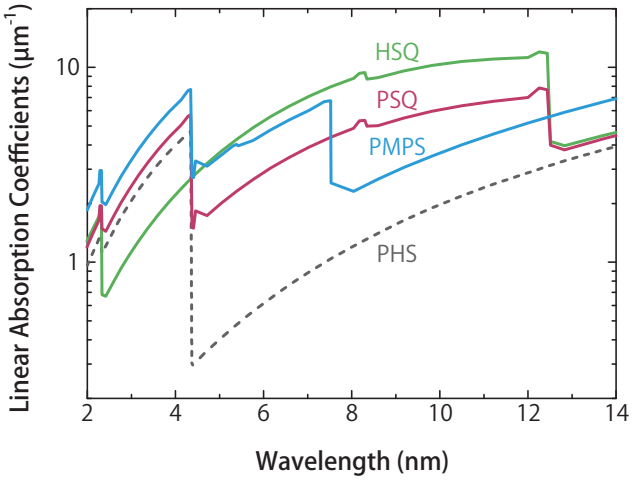

Fig. 2.3 | Calculated linear absorption coefficients of HSQ, PSQ, PMPS, and PHS.

Table 2.2 | Comparison of linear absorption coefficients.[55)]

Wavelength	Linear absorption coefficients (α)					
	ZEP	PMMA	PHS	HSQ	PSQ	PMPS
3.9 nm	5.38	2.87	3.77	2.10	4.52	6.09
6.7 nm	**1.08**	**0.79**	**0.79**	**6.54**	**3.55**	**5.52**
13.5 nm	4.59	1.79	3.65	4.31	4.19	6.41

2.3.2 Experimental evaluation of resist sensitivities

An experimental evaluation was conducted to validate the above prediction for resist sensitivities. The resist sensitivities for 6.7 nm EUV were investigated and compared with those for other wavelengths (p. 46) and the predicted values. Figure 2.4 shows the obtained sensitivity curves for ZEP resists, PMMA, and HSQ.

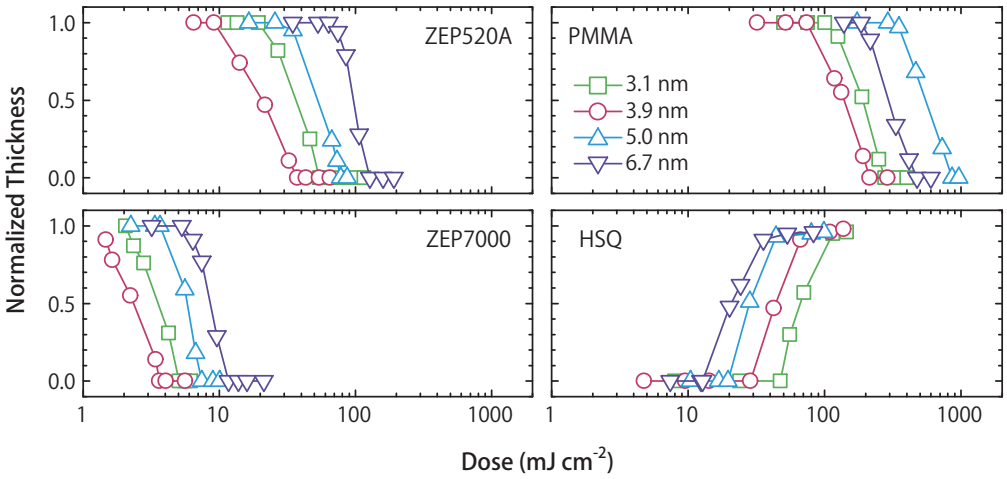

Fig. 2.4 | Sensitivity curves for EUV/soft X-rays including wavelength of 6.7 nm.

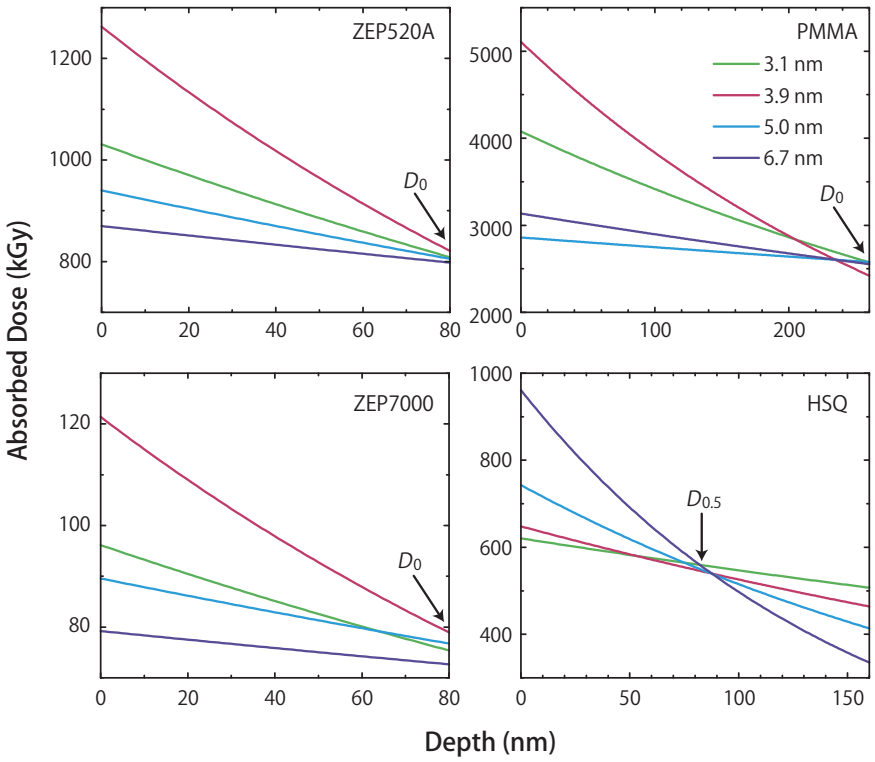

Fig. 2.5 | Calculated absorbed dose in ZEP resists, PMMA, and HSQ.

As shown in Fig. 2.5, the absorbed dose for sensitivity (D_0) was almost constant for each resist. In the case of the negative-tone resist HSQ, the sensitivity is defined as the dose at which the curve is at 50% of the film thickness ($E_{0.5}$). The absorbed doses corresponding to $E_{0.5}$ ($D_{0.5}$) of HSQ were nearly independent of the EUV/soft

X-ray wavelength.

The obtained sensitivities are compared with the predicted ones in Table 2.3. Both the obtained and predicted values agreed well, thereby confirming the validity of the prediction. The predictions for resist sensitivity demonstrated here can aid the selection or development of resists.

Table 2.3 | Comparison of obtained sensitivities with predicted ones.

	E_0 or $E_{0.5}$ (mJ cm^{-2})			
	ZEP520A	ZEP7000	PMMA	HSQ
Predicted	130	12	470	–
Obtained	129	11	476	20

2.4 Summary

In this chapter, we evaluated the resist sensitivity in the EUV/soft X-ray region for use in next-generation EUV lithography. As described in Chap. 4 of Part I, it was confirmed that each resist had a particular value of the required absorbed dose, regardless of exposure wavelength. On the basis of this result, once the resist sensitivities for a certain wavelength are experimentally obtained, those for other exposure wavelengths can be estimated. For example, materials containing sulfur and/or silicon, such as HSQ, PSQ and PMPS, are promising candidates for high sensitivity resists for 6.x nm EUV lithography.

The sensitivities of ZEP resists, PMMA, and HSQ were actually measured with 6.7 nm EUV/soft X-ray source. The obtained results agreed well with the predicted sensitivities. ZEP7000 and HSQ exhibited high sensitivities to 6.x nm EUV in this study. In addition, the results suggest that HSQ, PSQ, and PMPS can exhibit comparable sensitivities for use in lithography with wavelength of 6.7 nm to 13.5 nm.

The predictions of resist sensitivity demonstrated here will be very useful for the selection or development of high sensitivity resists, including CA ones. However, sensitivity for actual fabrication (E_{size}) should be considered for practical lithography. This will be the subject of a future.

3

X-ray Imaging with Resists for Elemental Mapping

X-ray microscopy has been considered a promising analytical tool for observation at the nano-scale spatial resolution. However, the spatial resolution of currently available monitoring devices, such as CCD cameras and imaging plates, are not sufficient for use in nano-scale imaging.

In this chapter, we report the use of ZEP resists for X-ray imaging. By placing a resist behind the object and irradiating with X-rays, the object's profile and X-ray absorption information can be recorded in the resist as the pattern and its depth. Using this approach, X-ray images of silicon nitride particles are successfully obtained with nanometer-order spatial resolution. Moreover, the principle of elemental mapping using monochromated X-rays is experimentally proved. The obtained results demonstrate the great potential of using resists as the detection layer in both nano-scale X-ray imaging and elemental mapping.

3.1 Introduction

Observation techniques with nano-scale spatial resolution have attracted considerable attention for use in various research fields such as material, chemical and biological sciences. X-ray microscopy is considered a promising analytical tool for such nano-scale observation; the characteristics of X-rays, which are listed below, offer several advantages over currently used observation techniques.[61)]

Short Wavelength

- Spatial resolution using X-ray is between those of optical and electron microscopes.

High Transparency

- Thick specimens (1–10 μm) can be observed without microtoming.
- 3-D observations such as computed tomography (CT) can be realized.

Distinct Absorption Edge

- Staining is not required because of the high contrast.
- Distribution of specific elements can be visualized.

Hence, X-ray microscopy can be used to realize 2-D or 3-D observations of samples in their natural state at a nano-scale resolution; further, the elemental mapping within these samples can be visualized.

Of particular interest for X-ray microscopy is the soft X-ray region between the K-shell absorption edges of carbon (4.37 nm/284 eV) and oxygen (2.33 nm/532 eV), known as the “water window”. In this region, the absorption coefficient of water is much lower than those of biologically and chemically important elements such as carbon and nitrogen. Hence, X-ray analysis using the water window X-rays enables the carbon/nitrogen elemental mapping of wet materials such as cells and biopolymers without requiring dehydration of samples.[61)]

Subsequent to W. C. Roentgen’s historic discovery of X-rays in 1895, many researchers have focused on the development of X-ray microscopy. Several kinds of imaging modes have been already established including projection and scanning, in combination with condensing and objective X-ray optics such as zone plates.[62–64)] However, the transmission efficiency of these devices for soft X-rays is very low (approximately 10%) due to high absorption, and consequently, the number of photons are eventually reduced to less than 1% of the original. Therefore, a very powerful soft X-ray source is required for projection or scanning microscopy.

On the other hand, contact imaging is a simple technique that requires no optical devices. In principle, it enables larger imaging fields with shorter exposure times

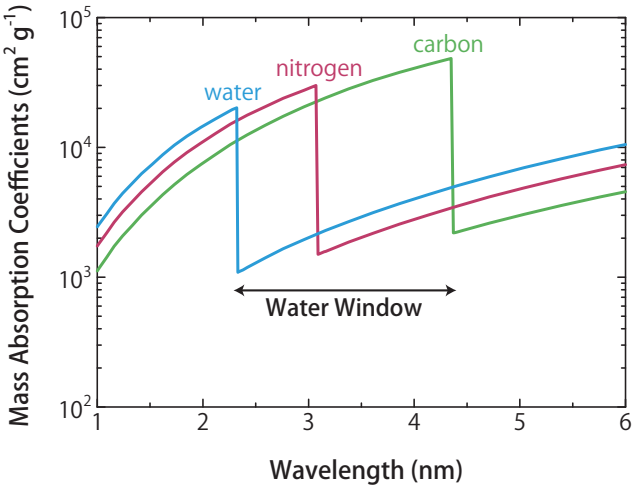

Fig. 3.1 | Water window X-ray region.[55)]

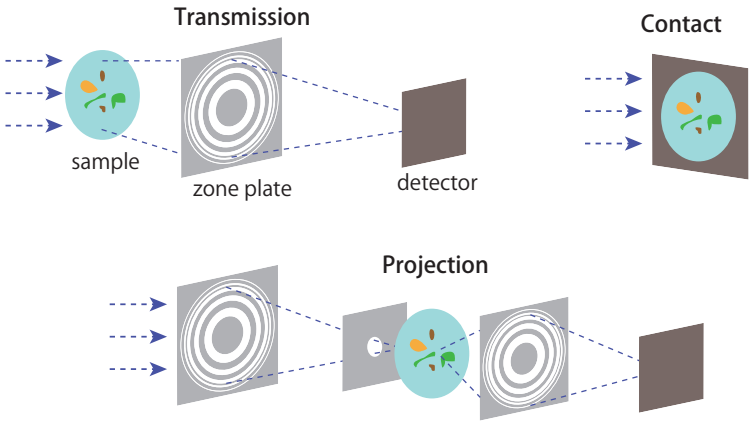

Fig. 3.2 | Typical X-ray imaging systems used in X-ray microscopy.

when compared with other observational modes.[61)] Moreover, this approach is better suited for high resolution imaging because it does not require optical devices which limit the final resolution. The only drawback of this approach is that the spatial resolution of currently available monitoring devices, such as CCD cameras and imaging plates, are not sufficient for nano-scale imaging.

Therefore, the use of high resolution resists as a detection layer for imaging has been considered as an alternative approach to realize nano-scale X-ray imaging. By placing a resist behind the object and irradiating with X-rays, the object's profile and X-ray absorption information can be recorded in the resist as the imaged pattern and its depth.[65)] The spatial resolution of the resist, which can be as high as 10 nm, is critical for achieving high spatial resolution X-ray microscopy.[66)] Therefore, nano-

scale imaging and elemental mapping can be realized by choosing appropriate X-ray wavelengths and examining the resist surface with a suitable profilometer such as an atomic force microscope (AFM).

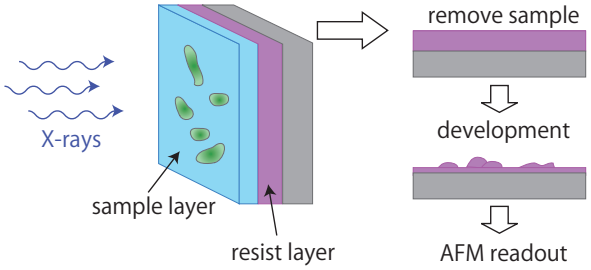

Fig. 3.3 | Contact X-ray microscopy with resists.

Tomie *et al.* employed AFM to read out the recorded pattern on PMMA, and they imaged living sperm in water.[67] Other studies have reported X-ray imaging with PMMA by using synchrotron radiation (SR) and laser plasma X-ray sources.[65,68] However, the primary challenge is the required high irradiation dose. This because the sensitivity of PMMA is very low, although its resolution is known to be as high as 10 nm. In consideration of radiation damage that can occur in the objects during imaging, it is required to choose resists with high sensitivity to minimize the irradiation dose. With resists with higher sensitivity, the X-ray flux and irradiation time can be reduced, and can be obtained using laboratory-type compact light sources such as inverse Compton X-rays,[69] further , the effects of image blurring can also be reduced.

As described in Part I Chap. 1, ZEP resists have an excellent spatial resolution better than 10 nm, and this is comparable to that of PMMA; further, the sensitivities of ZEP resists are much higher than than PMMA as mentioned in Chap. 4 of Part I. In addition, the predicted and obtained values of ZEP resist sensitivities to specific exposure wavelengths showed good agreement, as reported in Part II Chap. 2.

In this chapter, we evaluate the use of ZEP7000 in X-ray imaging towards the toward mapping of specific elements.

3.2 Methods

Sample preparation

Spin-coated ZEP7000 prepared by the standard procedure described in p. 16. The thickness of the ZEP7000 films after the pre-bake was approximately 150 nm.

Silicon nitride (Si_3N_4) powder with an average size of 65 nm (Wako) was mixed in the water-soluble polymer, Espacer 300 (Showa Denko K. K.), which is as antistatic

agent often used in EB lithography. Subsequently, this polymer was spin-coated on resist surface at 1000 rpm for 90 s. The thickness of this sample layer was approximately 40 nm. Before development, the sample layer (particles and Espacer) was completely removed using deionized water.

Soft X-ray irradiation, measurements, and simulations

The EUV/soft X-ray irradiation, measurements, and simulations were all conducted as described in Chap. 4 (p. 45).

3.3 Results and Discussion

The field emission scanning electron microscope (FE-SEM, S-4500S, HITACHI) image of the silicon nitride particles coated on ZEP7000 is shown in Fig. 3.4.

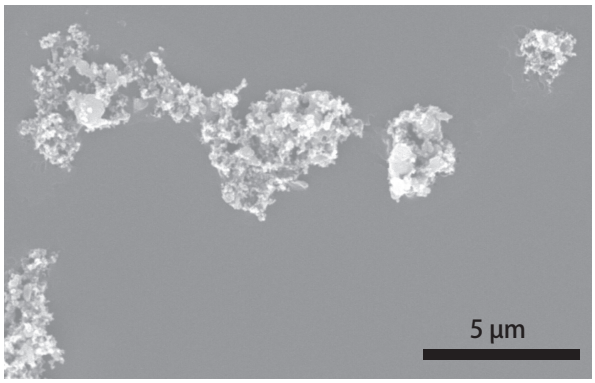

Fig. 3.4 | FE-SEM image of coated silicon nitride particles on ZEP7000.

As shown in Fig. 3.5, the absorption of silicon nitride drastically changes at the X-ray wavelength of around 3 nm, reflecting the K-shell absorption edge of nitrogen. On the other hand, it is to be noted that ZEP does not contain nitrogen atoms; this implies that the silicon nitride particles were imaged accurately.

The X-ray imaging of silicon nitride particles was attempted using 2.9 and 3.1 nm X-rays. The irradiated dose was about twice the dose for sensitivity. The results of the imaging are shown in Fig 3.6. Upon comparing the AFM images with the FE-SEM image in Fig. 3.4, it is observed that ab accurate X-ray image with nano-order resolution was successfully obtained on the ZEP7000 resist. The precise evaluation of the spatial resolution was difficult because the particles were agglutinated. However, considering that the resolutions of X-ray CCD and imaging plate are in micrometer range, this obtained result clearly shows the advantage of using resist as the detection layer.

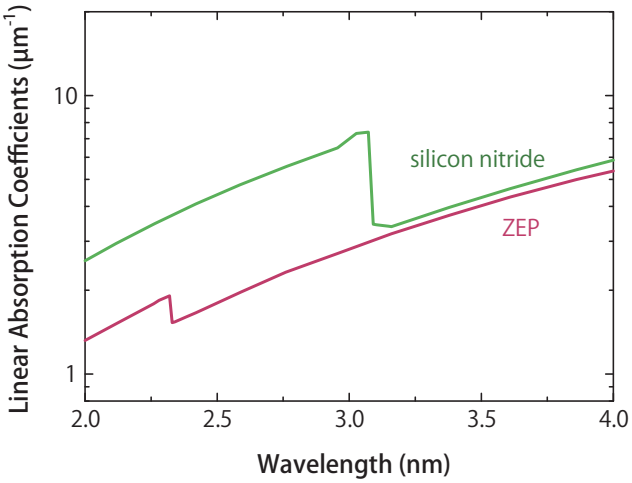

Fig. 3.5 | X-ray absorption of silicon nitride and ZEP.

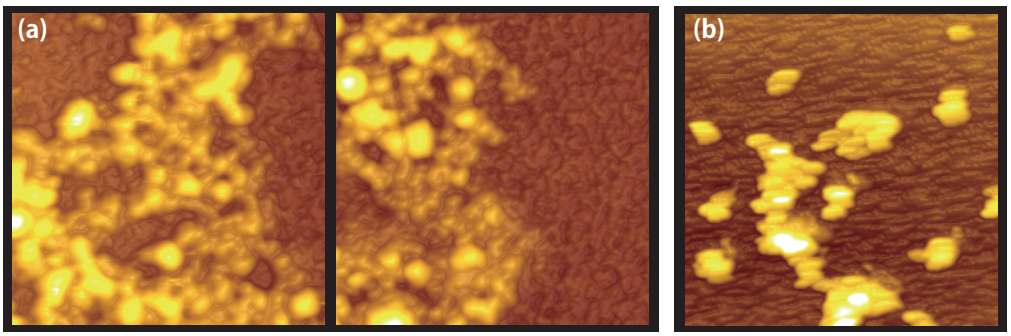

Fig. 3.6 | First X-ray imaging of silicon nitride particles with (a) 2.9 nm and (b) 3.1 nm soft X-rays. (AFM images, 5 μm squares)

Moreover, the resolution of the image obtained with the 3.1 nm X-ray was obviously less than that of the image obtained using the 2.9 nm X-ray. This is attributed to the low contrast resulting from lower absorption of silicon nitride in the former case. This result demonstrates the principle of elemental mapping using monochromated X-rays.

3.4 Summary

In this chapter, the application of high resolution resists as the detection layer for X-ray imaging was studied to realize elemental mapping. The doses required for the imaging were predicted as described in Part II Chap. 2, and X-ray images of silicon nitride nanoparticles were successfully obtained with nanometer-order spatial

resolution. Moreover, the principle of elemental mapping using monochromated X-rays was experimentally demonstrated. The obtained results highlight the potential use of resists as the detection layer in both nano-scale X-ray imaging and elemental mapping.

The next challenges in this area of research are the precise evaluation of the spatial resolution of X-ray imaging using ZEP7000, and X-ray imaging of wet samples such as cells.

Concluding Remarks

Conclusions

This dissertation described quantum-beam induced reactions in resists, particularly chlorinated resist ZEP (1:1 copolymers of α-chloromethacrylate and α-methylstyrene). The quantum-beam-induced reaction mechanisms of ZEP resists were discussed based on the analyses of the obtained final products and evaluations of resist performance.

The decomposition mechanisms of ZEP resists were precisely investigated. It was confirmed that chlorine atoms easily dissociated as Cl^- ions (DEA), and ZEP resists underwent β-scission. Multiple reaction channels were considered for the main-chain scission in ZEP, including DEA and CT complexes between phenyl rings and chlorine atoms. The obtained results provided some clues regarding the reason for the excellent balance between high resolution and high sensitivity of ZEP resists.

On the other hand, it was observed that the ZEP resists changed from positive-tone to negative-tone by high-dose irradiation of quantum beams (P-N inversion). P-N inversion is induced because chlorines are eliminated from the resists, and because of crosslinking, which was confirmed by the decrease in the number of terminal double bonds that formed via main-chain scission. Upon high-dose irradiation, the structural changes and the lower scission rate due to the decreased amount of chlorine change the ZEP resists into negative-tone. This is because the content of chlorines in the ZEP resists determines the threshold of P-N inversion.

The LET effects on resist performance were also investigated. The sensitivities varied, and less dose was required for higher LET. The calculated absorbed dose was constant for low-LET EBs; however, it was observed that the required absorbed doses increased for high LET ion beams. The possible reasons for the degraded sensitivities for high-LET beams would be low probability of main-chain scission, radical recombination, and inter/intra-molecular crosslinking.

In the case of photons such as EUV and X-rays, the absorption of incident radiation in the resists is an important factor in determination of resist sensitivity. The obtained sensitivities varied with the exposure wavelength, and it was experimentally confirmed that the absorption of the resists has a strong influence on the sensitivity. However, it was confirmed that the absorbed dose (given in Gy = J kg^{-1}), calculated from the dose/sensitivity curves and the respective linear absorption coefficient, was almost independent of the wavelength and constant for each resist. For low-LET quantum beams including EBs and EUV/soft X-rays, each resist had a particular value of the required absorbed dose, regardless of the irradiation source and wavelength.

In Part II of this dissertation, applications involving the use of ZEP resists to advanced technologies were demonstrated by controlling the quantum-beam-induced reactions discussed in Part I.

(1) By controlling the P-N inversion of ZEP resists in combination with control of the three-dimensional energy deposition distribution of the quantum beam, a novel micro/nanofabrication technique named the “nanobead from nanocup” was developed. The desired micro/nanostructures such as sub-millimeter-length wires and nanomembranes were obtained.

(2) The resist sensitivities were predicted on the basis of the result that each resist had a particular value of required absorbed dose for EUV/soft X-rays. The sensitivities were actually measured, and the obtained results agreed well with the predicted sensitivities. Moreover, the absorbed dose for EUV/soft X-rays was almost comparable to that for EBs. Hence, resist sensitivity for EUV/soft X-rays can be speculated by using the obtained sensitivity for EBs. The predictions of resist sensitivity can be very useful for the selection or development of high sensitivity resists for next-generation EUV lithography.

(3) The high resolution resists were applied as detection layers for X-ray imaging in order to realize elemental mapping. The required doses could predicted as described above, and X-ray imaging of nanoparticles was attempted using ZEP7000. The obtained results demonstrated the potential use of resists as the detection layer in both nano-scale X-ray imaging and elemental mapping.

This dissertation focused on the analyses of the obtained final products and resist performances to investigate the quantum-beam-induced reaction mechanisms. In order to grasp the entire context of the reactions, we also need to understand the early processes that determine the chemical reactions to form the final products. In addition, the resist sensitivity for actual fabrication (E_{size}) and the reaction mechanisms of CA-resists should be considered for practical lithography. These will form the topics of future studies.

Bibliography

1) G. E. Moore, "Cramming more components onto integrated circuits," *Electronics*, 38, 114–117, 1965.

2) G. E. Moore, "Progress in digital integrated electronics," in *International Electron Devices Meeting Technical Digest, IEEE*, 20, 11–13, 1975.

3) Intel Co., "Intel (http://www.intel.com/)."

4) B. La Fontaine, "Lasers and Moore's law," *SPIE Professional*, 2010.

5) The International Technology Roadmap for Semiconductors (ITRS), "ITRS (http://www.itrs.net/)."

6) T. Palacios, "Applied physics: Nanowire electronics comes of age," *Nature*, 481, 152–153, 2012.

7) The National Institute of Standards and Technology (NIST), "NIST standard reference database 111 (http://www.nist.gov/srd/)."

8) Y. Tabata, S. Tagawa, and M. Washio, "Pulse radiolysis studies on the mechanism of the high sensitivity of chloromethylated polystyrene as an electron negative resist," in *Materials for microlithography (ACS symposium series, 266)* (L. F. Thompson, C. G. Willson, and J. M. J. Fréchet, eds.), ch. 5, 151–163, Washington, D.C.: American Chemical Society, 1985.

9) S. Tagawa, "Pulse radiolysis and laser photolysis studies on radiation resistance and sensitivity of polystyrene and related polymers," *Int. J. Radiat. Appl. Instrum. C. Radiat. Phys. Chem.*, 27 (6), 455–459, 1986.

10) S. Tagawa, "Main reactions of chlorine- and silicon-containing electron and deep-UV (excimer laser) negative resists," in *Polymers for high technology (ACS symposium series, 346)* (M. J. Bowden and S. R. Turner, eds.), ch. 4, 37–45, Washington, D.C.: American Chemical Society, 1987.

11) S. Tagawa, "Pulse radiolysis studies of polymers," in *Radiation effects on polymers (ACS symposium series, 475)* (R. L. Clough and S. W. Shalaby, eds.), ch. 1, 2–30, Washington, D.C.: American Chemical Society, 1991.

12) T. Kozawa, Y. Yoshida, M. Uesaka, and S. Tagawa, "Radiation-induced acid generation reactions in chemically amplified resists for electron beam and X-ray lithography," *Jpn. J. Appl. Phys.*, 31, 4301–4306, 1992.

13) T. Kozawa and S. Tagawa, "Radiation Chemistry in Chemically Amplified Resists," *Jpn. J. Appl. Phys.*, 49, 030001-1–030001-19, 2010.

14) H. Ito, "Chemical amplification resists for microlithography," *Adv. Polymer. Sci.*, 37–245, 2005.

15) F. Emoto, K. Gamo, S. Namba, N. Samoto, and R. Shimizu, "8 nm wide line fabrication in PMMA on Si wafers by electron beam exposure," *Jpn. J. Appl. Phys.*, 24, L809–L811, 1985.

16) D. R. S. Cumming, S. Thoms, S. P. Beaumont, and J. M. R. Weaver, "Fabrication of 3 nm wires using 100 keV electron beam lithography and poly(methyl methacrylate) resist," *Appl. Phys. Lett.*, 68 (3), 322–324, 1996.

17) M. A. Mohsin and J. M. G. Cowie, "Enhanced sensitivity in the electron beam resist poly (methyl methacrylate) using improved solvent developer," *Polymer*, 29, 2130–2135, 1988.

18) S. Matsui, Y. Kojima, Y. Ochiai, and T. Honda "High-resolution focused ion beam lithography," *J. Vac. Sci. Tech. B.*, 9, 2622–2632, 1991.

19) H. Ito, C. G. Willson, and J. M. J. Fréchet, "New UV resists with negative or positive tone," *Digest of technical papers of 1982 symposium on VLSI technology*, 86–87, 1982.

20) H. Ito and C. G. Willson, "Chemical amplification in the design of dry developing resist materials," *Polymer. Eng. Sci.*, 23, 1012–1018, 1983.

21) K. Suyama and M. Shirai, "Photobase generators: Recent progress and application trend in polymer systems," *Progr. Polymer. Sci.*, 34, 194–209, 2009.

22) K. Kurihara, K. Iwadate, H. Namatsu, M. Nagase, H. Takenaka, and K. Murase, "An electron beam nanolithography system and its application to Si nanofabrication," *Jpn. J. Appl. Phys.*, 34, 6940–6946, 1995.

23) T. Nishida, M. Notomi, R. Iga, and T. Tamamura, "Quantum wire fabrication by e-beam elithography using high-resolution and high-sensitivity e-beam resist ZEP-520," *Jpn. J. Appl. Phys.*, 31, 4508–4514, 1992.

24) T. Yamaguchi, K. Yamazaki, and H. Namatsu, "Influence of molecular weight of resist polymers on surface roughness and line-edge roughness," *J. Vac. Sci. Tech. B.*, 22 (6), 2604–2610, 2004.

25) ZEON, "ZEP520 High resolution positive electron beam resist technical report, Ver.1.01," tech. rep., 2003.

26) ZEON, "ZEP7000 High resolution positive electron beam resist technical report, Ver.1.07," tech. rep., 2003.

27) H. Hirayama, Y. Namito, A. Bielajew, S. Wilderman, and W. Nelson, "The EGS5 code system.," SLAC Report number: SLAC-R-730, KEK Report number: 2005-8, 2010.

28) R. M. Silverstein, F. X. Webster, and D. J. Kiemle, *Spectrometric identification of organic compounds.* Hoboken, NJ: John Wiley & Sons, 7 ed., 2005.

29) U. Sevil, O. Güven, and S. Süzer, "Spectroscopic investigation of onset and enhancement of electrical conductivity in PVC/PANI composites and blends by γ-ray or UV irradiation," *J. Phys. Chem. B.*, 102 (20), 3902–3905, 1998.

30) B. Mutel, J. Grimblot, O. Dessaux, and P. Goudmand, "XPS investigations of nitrogen-plasma-treated polypropylene in a reactor coupled to the spectrometer," *Surf. Interface. Anal.*, 30 (1), 401–406, 2000.

31) A. P. Terzyk, "The influence of activated carbon surface chemical composition on the adsorption of acetaminophen (paracetamol) in vitro: Part II. TG, FTIR, and XPS analysis of carbons and the temperature dependence of adsorption kinetics at the neutral pH," *Colloids Surf., A*, 177 (1), 23–45, 2001.

32) K. Artyushkova and J. E. Fulghum, "Quantification of PVC-PMMA polymer blend compositions by XPS in the presence of x-ray degradation effects," *Surf. Interface. Anal.*, 31, 352–361, 2001.

33) M. Şen, B. Yolaçan, and O. Güven, "Radiation-induced degradation of galactomannan polysaccharides," *Nucl. Instr. Meth. Phys. Res. B*, 265, 429–433, 2007.

34) K. Dawes, L. Glover, and D. Vroom, "The effects of electron beam and γ-irradiation on polymeric materials," in *Physical properties of polymers handbook* (J. E. Mark, ed.), ch. 52, 867–887, New York: Springer, 2 ed., 2007.

35) J. N. Helbert, G. J. Iafrate, C. U. Pittman Jr, and J. H. Lai, "Effect of chemical composition upon the radiation and electron beam resist behaviors of vinyl polymers," *Polym. Eng. Sci.*, 20 (16), 1077–1081, 1980.

36) C. G. Willson, H. Ito, D. C. Miller, T. G. Tessier, and S. Jose, "Poly(methyl α-trifluoromethylacrylate) as a positive electron beam resist," *Polymer. Eng. Sci.*, 23 (18), 1–4, 1983.

37) H. Kudoh, M. Celina, G. Malone, R. Kaye, K. Gillen, and R. Clough, "Pulsed e^- beam irradiation of polymers – A comparison of dose rate effects and LET effects," *Radiat. Phys. Chem.*, 48, 555–562, 1996.

38) S. Beavan and W. Schnabel, "On the kinetics of polymer degradation in solution. 8. Laser flash photolysis of polystyrene," *Macromolecules*, 11 (4), 782–785, 1978.

39) S. Tagawa and W. Schnabel, "Laser flash photolysis studies on excited singlet states of benzene, toluene, *p*-xylene, polystyrene, and poly-α-methylstyrene," *Chem. Phys. Lett.*, 75, 120–122, 1980.

40) S. Tagawa and W. Schnabel, "On the mechanism of the photolysis of polystyrene in chloroform solution. Laser flash photolysis studies," *Makromol. Chem., Rapid Commun.*, 1 (5), 345–350, 1980.

41) S. Tagawa, "On the kinetics of polymer degradation. X—Laser flash photolysis of poly-α-methylstyrene in chloroform solution," *Polym. Photochem.*, 3 (3), 203–209, 1983.

42) S. Tagawa, W. Schnabel, M. Washio, and Y. Tabata, "Picosecond pulse radiolysis and laser flash photolysis studies on polymer degradation of polystyrene and poly-α-methylstyrene," *Radiat. Phys. Chem.*, 18, (5–6), 1087–1095, 1981.

43) S. Tagawa, "Radiation effects of ion beams on polymers," in *Recent trends in radiation polymer chemistry* (S. Okamura, ed.), 105 of *Advances in polymer science*, 99–116, Springer Berlin / Heidelberg, 1993.

44) A. Oshima and M. Washio, "Radiation-induced phenomena in ethylene-co-tetrafluoroethylene polymer, Temperature and LET effects," *Nucl. Instr. Meth. Phys. Res. B*, 208, 380–384, 2003.

45) T. Gowa, T. Shiotsu, T. Urakawa, T. Oka, T. Murakami, A. Oshima, Y. Hama, and M. Washio, "Study on depth profile of heavy ion irradiation effects in poly(tetrafluoroethylene-co-ethylene)," *Radiat. Phys. Chem.*, 80, 264–267, 2011.

46) D. Drouin, P. Hovington, and R. Gauvin, "CASINO: A new Monte Carlo code in C language for electron beam interactions—Part II: Tabulated values of the Mott cross section," *Scanning*, 19, 20–28, 1997.

47) P. Hovington and D. Drouin, "CASINO: A new Monte Carlo code in C language for electron beam interaction—Part I: Description of the program," *Scanning*, 19, 1–14, 1997.

48) D. Drouin, A. Couture, D. Joly, X. Tastet, V. Aimez, and R. Gauvin, "CASINO V2.42—A fast and easy-to-use modeling tool for scanning electron microscopy and microanalysis users.," *Scanning*, 29 (3), 92–101, 2007.

49) J. F. Ziegler, J. P. Biersack, and M. D. Ziegler, "SRIM-2011, the stopping and range of ions in matter (http://www.srim.org)," 2011.

50) T. Kozawa and S. Tagawa, "Radiation chemistry of resist materials and processes in lithography," in *Charged particle and photon interactions with matter: Recent advances, applications, and interfaces* (Y. Hatano, Y. Katsumura, and A. Mozumder, eds.), ch. 26, 711–736, CRC Press, 2011.

51) T. Kozawa, S. Tagawa, H. Oizumi, and I. Nishiyama, "Acid generation efficiency in a model system of chemically amplified extreme ultraviolet resist," *J. Vac. Sci. Tech. B.*, 24 (6), L27–L30, 2006.

52) H. Yamamoto, T. Kozawa, S. Tagawa, H. B. Cao, H. Deng, and M. J. Leeson, "Polymer-structure dependence of acid generation in chemically amplified extreme ultraviolet resists," *Jpn. J. Appl. Phys.*, 46, L142–L144, 2007.

53) H. Yamamoto, T. Kozawa, S. Tagawa, H. Yukawa, M. Sato, and J. Onodera, "Enhancement of acid production in chemically amplified resist for extreme ultraviolet lithography," *Appl. Phys. Express.*, 1, 047001-1–047001-3, 2008.

54) RIKEN/JASRI, "SPring-8 (http://www.spring8.or.jp/)."

55) The National Institute of Standards and Technology (NIST), "NIST standard reference database 66 (http://www.nist.gov/srd/)."

56) T. G. Oyama, A. Oshima, M. Washio, and S. Tagawa, "Evaluation of resist sensitivity in extreme ultraviolet/soft x-ray region for next-generation lithography," *AIP Adv.*, 1 (4), 042153-1–042153-5, 2011.

57) T. Tsarfati, R. W. E. van de Kruijs, E. Zoethout, E. Louis, and F. Bijkerk, "Reflective multilayer optics for 6.7nm wavelength radiation sources and next generation lithography," *Thin Solid Films*, 518, 1365–1368, 2009.

58) H. Meiling, "EUVL-getting ready for volume introduction," in *SEMICON West 2010*, 2010.

59) J. Benschop, "EUV: Status and challenges ahead," in *International workshop on EUVL*, keynote-1, 2010.

60) V. Banine, A. Yakunin, and D. Glushkov, "Next generation EUV lithography: Challenges and opportunities," in *2010 International workshop on extreme ultraviolet sources*, 14, 2010.

61) J. Kirz, C. Jacobsen, and M. Howells, "Soft x-ray microscopes and their biological applications," *Q. Rev. Biophys.*, 28 (01), 33–130, 1995.

62) J. Kirz and C. Jacobsen, "The history and future of X-ray microscopy," *J. Phys. Conf.*, 186, 012001-1–012001-11, 2009.

63) W. Chao, B. D. Harteneck, J. A. Liddle, E. H. Anderson, and D. T. Attwood, "Soft X-ray microscopy at a spatial resolution better than 15 nm.," *Nature*, 435, 1210–1213, 2005.

64) A. Sakdinawat and D. Attwood, "Nanoscale X-ray imaging," *Nat. Photon.*, 4, 840–848, 2010.

65) Y. Yamamoto and K. Shinohara, "Application of X-ray microscopy in analysis of living hydrated cells.," *Anat. Rec.*, 269, 217–23, 2002.

66) D. Sayre and H. N. Chapman, "X-ray microscopy," *Acta Crystallogr. Sect. A*, 51, 237–252, 1995.

67) T. Tomie, H. Shimizu, T. Majima, M. Yamada, T. Kanayama, H. Kondo, M. Yano, and M. Ono, "Three-dimensional readout of flash x-ray images of living sperm in water by atomic-force microscopy.," *Science*, 252, 691–693, 1991.

68) J. Wm. McGowan, B. Borwein, J. A. Medeiros, T. Beveridge, J. D. Brown, E. Spiller, R. Feder, J. Topalian, and W. Gudat, "High resolution microchemical analysis using soft x-ray lithographic techniques.," *J. Cell. Biol.*, 80 (3), 732–735, 1979.

69) K. Sakaue, T. Gowa, H. Hayamo, Y. Kamiya, S. Kashiwagi, R. Kuroda, A. Masuda, R. Moriyama, J. Urakawa, K. Ushida, X. Wang, and M. Washio, "Recent progress of a soft X-ray generation system based on inverse Compton scattering at Waseda University," *Radiat. Phys. Chem.*, 77, 1136–1141, 2008.

Publications

Peer-Reviewed Papers

Journal articles

- **T. G. Oyama**, A. Oshima, M. Washio, and S. Tagawa, “Evaluation of resist sensitivity in the exposure wavelength of 6.x nm for next-generation extreme ultraviolet lithography", *AIP Advances.* 1, 042153-1–042153-6, 2011.
- **T. G. Oyama**, A. Oshima, H. Yamamoto, S. Tagawa, and M. Washio, “Study on positive–negative inversion of chlorinated resist materials", *Appl. Phys. Express.*, 4, 076501-1–076501-3, 2011.
- **T. Gowa**, T. Takahashi, A. Oshima, S. Tagawa, and M. Washio, “Study on resist sensitivities for nano-scale imaging using water window X-ray microscopy", *Radiat. Phys. Chem.*, 80 (2), 248–252, 2011.
- **T. Gowa**, T. Shiotsu, T. Urakawa, T. Oka, T. Murakami, A. Oshima, Y. Hama, and M. Washio, “Study on depth profile of heavy ion irradiation effects in poly(tetrafluoro-ethylene-co-ethylene)", *Radiat. Phys. Chem.*, 80 (2), 264–267, 2011.
- A. Oshima, S. Okubo, **T. G. Oyama**, M. Washio, and S. Tagawa, “Nano-and Microfabrications of Polystyrene Having Atactic and Syndiotactic Structures using Focused Ion Beams Lithography”, *Radiat. Phys. Chem.*, In Press
- H. Tsubokura, A. Oshima, **T. G. Oyama**, H. Yamamoto, T. Murakami, S. Tagawa, and M. Washio, “Nanofabrication of sulfonated polystyrene-g-FEP with silver ion (Ag^+) using ion beam direct etching and reduction", *J. Photopolym. Sci. Technol.*, 24 (5), 513–516, 2011.
- T. Takahashi, Y. Hirano, Y. Takasawa, **T. Gowa**, N. Fukutake, A. Oshima, S. Tagawa, and M. Washio, “Change in surface morphology of polytetrafluoroethylene by reactive ion etching", *Radiat. Phys. Chem.*, 80 (2), 253–256, 2011.
- N. Miyoshi, A. Oshima, T. Urakawa, N. Fukutake, H. Nagai, **T. Gowa**, Y. Takasawa, T. Takahashi, Y. Numata, T. Katoh, E. Katoh, S. Tagawa, and M. Washio, “Nano- and micro-fabrication of perfluorinated polymers using quantum beam technology", *Radiat. Phys. Chem.*, 80 (2), 230–235, 2011.
- F. Shiraki, T. Yoshikawa, A. Oshima, Y. Oshima, Y. Takasawa, N. Fukutake, **T. G. Oyama**, T. Urakawa, H. Fujita, T. Takahashi, T. Oka, H. Kudo, T. Murakami, Y. Hama, and M. Washio, “Development of function-graded proton exchange membrane for PEFC using heavy ion beam irradiation", *Nucl. Instr. Meth. Phys. Res. B.*, 269, 1777–1781, 2011.

- **T. Gowa**, T. Takahashi, T. Oka, T. Murakami, A. Oshima, S. Tagawa, and M. Washio, “Ion beam irradiation effects on resist materials", *J. Photopolym. Sci. Technol.*, 23 (3), 399–404, 2010.
- T. Takahashi, Y. Takasawa, **T. Gowa**, S. Okubo, T. Sasaki, T. Miura, A. Oshima, S. Tagawa, and M. Washio, “Study on UV/EB nanoimprint lithography using nano-/micro-fabricated crosslinked PTFE mold", *J. Photopolym. Sci. Technol.*, 23 (1), 69–74, 2010.
- S. Okubo, T. Takahashi, **T. Gowa**, T. Sasaki, N. Nagasawa, M. Tamada, A. Oshima, S. Tagawa, and M. Washio, “Micro-fabrication of biodegradable polymers using focused ion beam", *J. Photopolym. Sci. Technol.*, 23 (3), 393–397, 2010.
- N. Fukutake, N. Miyoshi, Y. Takasawa, T. Urakawa, **T. Gowa**, K. Okamoto, A. Oshima, S. Tagawa, and M. Washio, “Micro- and nano-scale fabrication of fluorinated polymers by direct etching using focused ion beam", *Jpn. J. Appl. Phys.*, 49, 065201-1–065201-5, 2010.
- **T. Gowa**, N. Fukutake, Y. Hama, K. Hizume, T. Kashino, S. Kashiwagi, R. Kuroda, A. Masuda, A. Oshima, T. Saito, K. Sakaue, K. Shinohara, T. Takahashi, T. Urakawa, K. Ushida, and M. Washio, “Development of a compact X-ray source and super-sensiti-zation of photo resists for soft X-ray imaging", *J. Photopolym. Sci. Technol.*, 22 (3), 273–278, 2009.
- S. Kashiwagi, R. Kato, G. Isoyama, K. Sakaue, A. Masuda, T. Nomoto, **T. Gowa**, M. Washio, R. Kuroda, and J. Urakawa, “Development of compact coherent EUV source based on laser Compton scattering", *Radiat. Phys. Chem.*, 78 (12), 1112–1115, 2009.
- K. Sakaue, **T. Gowa**, H. Hayano, Y. Kamiya, S. Kashiwagi, R. Kuroda, A. Masuda, R. Moriyama, J. Urakawa, K. Ushida, X. Wang, and M. Washio, “Recent progress of a soft X-ray generation system based on inverse Compton scattering at Waseda University", *Radiat. Phys. Chem.*, 77 (10-12), 1136–1141, 2008.

Conference proceedings

- **T. G. Oyama**, T. Takahashi, A. Oshima, M. Washio, and S. Tagawa, “Extendibility of EUV resists in the exposure wavelength from 13.5 down to 3.1 nm for next-generation lithography", *Proc. SPIE*, 7972, 797210-1–797210-6, 2011.
- **T. Gowa**, Y. Kamiya, A. Masuda, R. Moriyama, K. Sakaue, M. Washio, R. Kuroda, S. Kashiwagi, H. Hayano, J. Urakawa, and K. Ushida, “Improvement of Soft X-ray Generation System Based on Laser Compton Scattering", *Proc. of Particle Accelerator Conference 2007*, TUPMN049, 1031–1033, 2007.

Conferences

Oral presentations

- **T. G. Oyama**, T. Takahashi, A. Oshima, M. Washio, and S. Tagawa, “Extendibility of EUV resists in the exposure wavelength from 13.5 down to 3.1 nm for next-generation lithography", SPIE Advanced Lithography, 7972-36, CA, USA (Mar. 2, 2011)
- **T. G. Oyama**, A. Oshima, H. Yamamoto, S. Tagawa, and M. Washio, “Positive-negative inversion of resist materials induced by high LET radiation", 9th Meeting of the Ionizing Radiation and Polymers Symposium, S9, Maryland, USA (Oct. 28, 2010)
- **T. Gowa**, T. Takahashi, T. Urakawa, N. Fukutake, K. Sakaue, A. Oshima, and M. Washio, “Study on sensitivities of resist materials under UV, EB and soft X-ray exposure", 11th Pacific Polymer Conference, 379, Cairns, Australia (Dec. 8, 2009)
- **五輪智子**、五十嵐千明、樫野多加志、加藤雄太、小宮圭太、坂上和之、鈴木達也、野本知章、濱義昌、藤田晃宏、増田明彦、村田亜希、鷲尾方一、浦川順治、早野仁司、黒田隆之助、柏木茂、丑田公規、X. J. Wang「早稲田大学 RF 電子銃における応用研究と将来計画」第 5 回高輝度高周波電子銃研究会 早稲田大学 (2007 年 12 月)
- **五輪智子**、五十嵐千明、樫野多加志、坂上和之、増田明彦、鷲尾方一、浦川順治、早野仁司、黒田隆之助、柏木茂、丑田公規「早稲田大学における逆コンプトン散乱を用いた水の窓軟Ｘ線源の開発」日本物理学会第 63 回年次大会 26aZL14、近畿大学 (2008 年 3 月）
- **五輪智子**、増田明彦、裏川達也、福武直之、坂上和之、篠原邦夫、濱義昌、鷲尾方一、大島明博、柏木茂、黒田隆之助、丑田公規「軟Ｘ線顕微鏡の開発に向けたフォトレジストを用いた撮像法の検討と評価」26th International Conference of Photopolymer Science and Technology 日本語講演 B5–01、千葉大学 （2009 年 7 月）
- **五輪智子**、高橋朋宏、岡壽崇、村上健、大島明博、田川精一、鷲尾方一「レジスト材料に対する各種イオンビーム照射効果に関する研究」27th International Conference of Photopolymer Science and Technology 日本語講演 B4–09、千葉大学（2010 年 6 月）

Poster presentations

- **T. G. Oyama**, H. Tsubokura, A. Oshima, S. Tagawa, and M. Washio, “Electron and ion beam fabrication using positive–negative inversion of chlorinated resist materials", 37th International Conference on Micro and Nano Engineering, Berlin, Germany (Sep. 21, 2011)

- **T. G. Oyama**, A. Oshima, S. Tagawa, and M. Washio, “X-ray Imaging with Resist Materials for Elemental Mapping", 14th International Congress of Radiation Research, Warsaw, Poland (Sep. 1, 2011)
- **T. G. Oyama**, H. Tsubokura, H. Yamamoto, A. Oshima, S. Tagawa, and M. Washio, “Positive–negative inversion of ZEP resists induced by high dose EB irradiation", Rad-Tech Asia 2011, P-41, Yokohama, Japan (Jun. 22, 2011)
- **T. G. Oyama**, A. Oshima, H. Yamamoto, S. Tagawa, and M. Washio, “Positive-negative inversion of resist materials induced by high LET radiation", 9th Meeting of the Ionizing Radiation and Polymers Symposium, Maryland, USA (Oct. 29, 2010)
- **T. Gowa**, T. Shiotsu, T. Urakawa, T. Oka, T. Murakami, A. Oshima, Y. Hama, and M. Washio, “Study on depth profile of heavy ion irradiation effects in poly(tetrafluoroethylene-co-ethylene)", 11th Pacific Polymer Conference, P254, Cairns, Australia (Dec. 8, 2009)
- **T. Gowa**, T. Kashino, A. Oshima, T. Urakawa, C. Igarashi, A. Masuda, K. Sakaue, Y. Hama, M. Washio, R. Kuroda, S. Kashiwagi, and Kiminori Ushida, “Evaluation of a chemically amplified photo resist for nanoscale soft X-ray imaging", 2nd Asia-Pacific Symposium on Radiation Chemistry, 1P–10, Tokyo, Japan (Aug. 30, 2008)
- **T. Gowa**, Y. Kamiya, A. Masuda, R. Moriyama, K. Sakaue, M. Washio, R. Kuroda, S. Kashiwagi, H. Hayano, J. Urakawa, and K. Ushida, “Improvement of soft X-ray generation system based on laser Compton scattering", Particle Accelerator Conference, TUPMN049, Albuquerque, USA (Jun. 26, 2007)

Others

Patent Application

- 特願 2011-052359 「微細加工体及びその製造方法」 鷲尾方一、**大山智子**、大久保聡、小林亜暢、高橋朋宏、大島明博、田川精一、長澤尚胤、田口光正

Awards

- “9th Meeting of the Ionizing Radiation and Polymers Symposium Student Award" (Oct. 28, 2010)
- “2nd Asia-Pacific Symposium on Radiation Chemistry Poster Award" (Sept. 1, 2008)
- 「早稲田大学理工学研究所創設 70 周年ポスターセッション Science 賞」 (Aug. 5, 2010)

Acknowledgments

I have had the privilege of studying with excellent supervisors — Prof. Masakazu Washio and Prof. Seiichi Tagawa. Along with their knowledge and experiences in the broad field of radiation physics and chemistry, they have always taught me the importance of studying with enjoyment. I am heartily thankful to Prof. Yoshimasa Hama and Prof. Yuka Tabe for their suggestions and encouragement.

I would like to acknowledge Dr. Akihiro Oshima for educating me from the very basics, Dr. Kazuyuki Enomoto, Dr. Hiroki Yamamoto, and Dr. Kazuyuki Sakaue for their advice and warm support. I am also grateful to Prof. Koji Arimitsu, Prof. Kunio Shinohara, Mr. Takashi Sasaki, Dr. Toshitaka Oka, Prof. Shigeru Kashiwagi, Dr. Ryunosuke Kuroda, and Dr. Masayuki Ito for inspiring my work.

I thank the faculty members of Washio Laboratory, and in particular, I would like to thank Mr. Ryo Moriyama, Mr. Akihiko Masuda, Mr. Yuta Kato, Ms. Aki Murata, Mr. Tomoaki Nomoto, Mr. Tatsuya Urakawa, Mr. Naoyuki Fukutake, Mr. Yuji Oshima, Mr. Takashi Kashino, Ms. Chiaki Kato, Mr. Fumiya Shiraki, Mr. Tatsuya Suzuki, Mr. Yuya Takasawa, Mr. Yuji Hosaka, Mr. Tomohiro Takahashi, Mr. Hajime Fujita, Mr. Satoshi Okubo, Mr. Hidehiro Tsubokura, Mr. Takahiro Tatsumi, Ms. Taeko Yoshikawa, Mr. Ryosuke Betto, Mr. Koichi Ogata, and Mr. Akinobu Kobayashi. It was a pleasure for me to work with you all.

My very special thanks go to Mr. Takaharu Miura, Ms. Ami Matsuo, and Ms. Kyoko Obama, who have always kept my spirits up. Also, I am grateful to golden girls who graduated from the Department of Physics together: Ms. Tomomi Abe, Ms. Risa Uratani, and Ms. Hiromi Niwa.

Here, I would like to use this opportunity to thank my family and friends, Eri, Ayako, and Chisato, for their warm support and understanding, even in hard times after the 3.11 disaster. Whatever happens, nothing beats Fukushima. Last but not least, none of this would have been possible without my dear husband Kotaro. You are my best collaborator, and you have helped me get to where I am now.

Tomoko GOWA OYAMA

This work was supported by Grant-in-Aid for JSPS Fellows 21-04550 (T. G. Oyama). A part of this work was conducted at Handai Multi-Functional Nanofoundry supported by “Nanotechnology Network Project” and Research Center for Organic/Oxide Green Nano Device (Osaka University) supported by ”Low-Carbon Research Network Project” of the Ministry of Education, Culture, Sports, Science and Technology (MEXT). The ion beam irradiation experiments were supported by the Research Project with Heavy Ions at NIRS-HIMAC (22P186). The synchrotron radiation experiments were performed at the BL27SU of SPring-8 with the approval of the Japan Synchrotron Radiation Research Institute (JASRI) (No. 2011B1369). A part of this work was supported by the RISE research project of Waseda University (11L01).